Article

Cell Reports

Epithelial WNT Ligands Are Essential Drivers of Intestinal Stem Cell Activation

Graphical Abstract

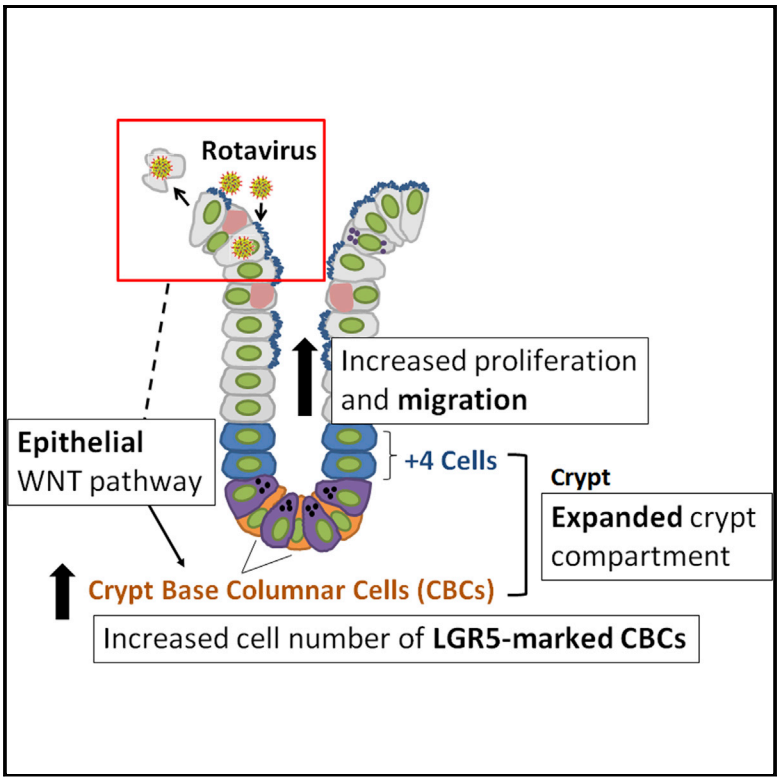

Authors

Winnie Y. Zou, Sarah E. Blutt, Xi-Lei Zeng, ..., Noah F. Shroyer, Mark Donowitz, Mary K. Estes

Correspondence

mestes@bcm.edu

In Brief

Using rotavirus infection as an intestinal epithelial injury model, Zou et al. demonstrate that crypt-based columnar cells are the predominant cell type responding to epithelial villus injury, and WNT ligands secreted from the intestinal epithelium are essential for this regenerative process.

Highlights

- Rotavirus infection is an excellent model for investigating intestinal villus injury
- Villus damage stimulates the active crypt-based columnar intestinal stem cells
- Reserve intestinal stem cells play a minimal role in repair of villus injury
- Regeneration following villus injury depends on epithelial-secreted WNT

Zou et al., 2018, Cell Reports 22, 1003–1015
January 23, 2018
https://doi.org/10.1016/j.celrep.2017.12.093

CellPress

Cell Reports
Article

Epithelial WNT Ligands Are Essential Drivers of Intestinal Stem Cell Activation

Winnie Y. Zou,[1] Sarah E. Blutt,[1] Xi-Lei Zeng,[1] Min-Shan Chen,[2] Yuan-Hung Lo,[2] David Castillo-Azofeifa,[4] Ophir D. Klein,[4] Noah F. Shroyer,[2] Mark Donowitz,[3] and Mary K. Estes[1,2,5,*]
[1]Department of Molecular Virology and Microbiology
[2]Section of Gastroenterology and Hepatology, Department of Medicine
Baylor College of Medicine, Houston, TX 77030, USA
[3]Division of Gastroenterology and Hepatology, Department of Medicine, Johns Hopkins University School of Medicine, Baltimore, MD 21218, USA
[4]Departments of Orofacial Sciences and Pediatrics, University of California, San Francisco, San Francisco, CA 94143, USA
[5]Lead Contact
*Correspondence: mestes@bcm.edu
https://doi.org/10.1016/j.celrep.2017.12.093

SUMMARY

Intestinal stem cells (ISCs) maintain and repair the intestinal epithelium. While regeneration after ISC-targeted damage is increasingly understood, injury-repair mechanisms that direct regeneration following injuries to differentiated cells remain uncharacterized. The enteric pathogen, rotavirus, infects and damages differentiated cells while sparing all ISC populations, thus allowing the unique examination of the response of intact ISC compartments during injury-repair. Upon rotavirus infection in mice, ISC compartments robustly expand and proliferating cells rapidly migrate. Infection results specifically in stimulation of the active crypt-based columnar ISCs, but not alternative reserve ISC populations, as is observed after ISC-targeted damage. Conditional ablation of epithelial WNT secretion diminishes crypt expansion and ISC activation, demonstrating a previously unknown function of epithelial-secreted WNT during injury-repair. These findings indicate a hierarchical preference of crypt-based columnar cells (CBCs) over other potential ISC populations during epithelial restitution and the importance of epithelial-derived signals in regulating ISC behavior.

INTRODUCTION

The small intestinal epithelium is one of the fastest renewing tissues in the human body, regenerating every 4–5 days (van der Flier and Clevers, 2009; Mezoff and Shroyer, 2015). This regenerative capacity is critical for maintaining the epithelium, protecting against constant insults from the luminal environment. Intestinal stem cells (ISCs) in the crypts maintain and repair the epithelial surface by giving rise to differentiated cells on the villi. Differentiation of ISCs in the crypts produces daughter cells that migrate up in a "conveyer belt" fashion to the villi, where they mature into both absorptive and secretory cells that play a major role in nutrient absorption and other intestinal functions (Potten, 1997; van der Flier and Clevers, 2009; Mezoff and Shroyer, 2015; Henning and von Furstenberg, 2016; Beumer and Clevers, 2016). One exception to this migratory pathway is the mature Paneth cells, which remain in the crypts instead of migrating upward, interact closely with the ISCs, and secrete stem cell maintenance factors, including WNT (Henning and von Furstenberg, 2016; Mezoff and Shroyer, 2015; Beumer and Clevers, 2016).

The crypts are thought to contain two types of ISCs (Henning and von Furstenberg, 2016; Mezoff and Shroyer, 2015; Beumer and Clevers, 2016). The best studied is the crypt-based columnar cells (CBCs) located at the base of the crypt. CBCs express the cell-surface marker leucine-rich repeat-containing G-protein-coupled receptor 5 (LGR5), among others, and continually proliferate under homeostasis (Cheng and Leblond, 1974a, 1974b; Barker et al., 2007). There is also evidence for an alternative reserve ISC population, which can be referred to as +4 cells or quiescent ISCs, as well as early absorptive and secretory progenitors that reside above the base of the crypt (Potten and Hendry, 1975; Potten, 1977; van der Flier and Clevers, 2009; Mezoff and Shroyer, 2015). Traditionally, tissue renewal after injury in the intestine has been studied using γ-irradiation, chemotherapy treatments, or genetic ablation, in which proliferating crypt-based columnar ISCs are ablated (Beumer and Clevers, 2016). CBC loss can activate reserve ISCs or the dedifferentiation of committed progenitors to repopulate the CBC pool and provide epithelial restoration (May et al., 2008; Potten et al., 2009; Takeda et al., 2011; Tian et al., 2011; Hua et al., 2012; Powell et al., 2012; van Es et al., 2012; Van Landeghem et al., 2012; Yan et al., 2012; Yu, 2013; Metcalfe et al., 2014; Poulin et al., 2014; Roche et al., 2015; Tetteh et al., 2016; Buczacki et al., 2013). These studies highlight the dynamic nature of the ISC niche that can readily regenerate following functional stem cell loss. However, while ISCs are well characterized under homeostatic conditions or situations where they are damaged directly, very little is known about the differential activation of these populations under intestinal epithelial dysbiosis in which ISCs remain undamaged.

The maintenance and regeneration of the intestinal epithelium is regulated, at least in part, by canonical WNT/β-catenin signaling (Clevers et al., 2014; Clevers and Nusse, 2012; Kühl

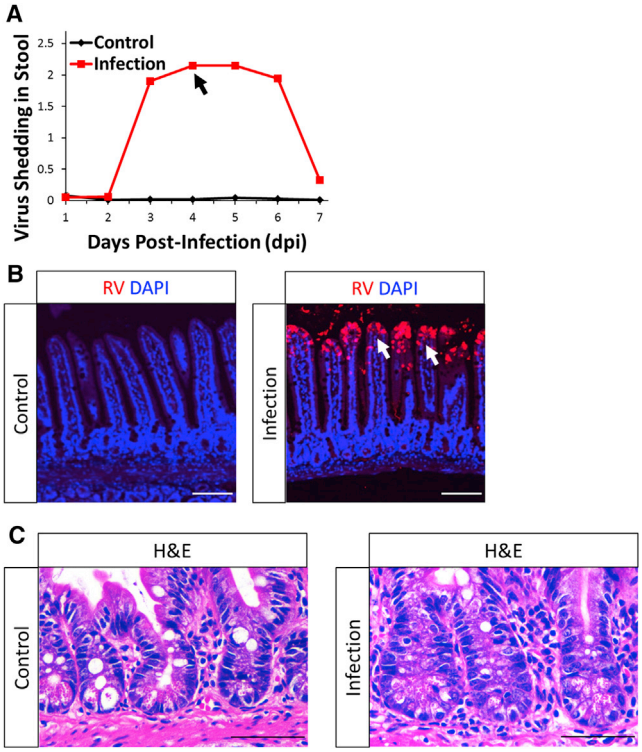

Figure 1. RV Infection Is Limited to the Tip of the Villi, Preserving an Intact Crypt Compartment

(A) Representative stool ELISA monitoring RV infections. Points represent means of respective groups (n = 2). Peak viral shedding was observed at 4 days post-infection (dpi; black arrow).

(B) Representative confocal images of control- and RV-infected mouse epithelium. RV-infected differentiated cells were detected using a laboratory-generated, polyclonal anti-RV antibody. Infected villi are noted by white arrows.

(C) Representative H&E images showing intact crypts in both control- and RV-infected mouse epithelium.

See also Figures S1 and S2.

and Kühl, 2013; Nusse and Varmus, 2012; Shroyer et al., 2015; Yan et al., 2017b). Extracellular WNT ligands bind to membrane Frizzled (FZD) receptors to trigger intracellular translocation of the transcriptional co-activator β-catenin, which can then drive the expression of well-established WNT pathway target genes (Nusse and Varmus, 2012). Studies in mice have indicated that cells in the intestinal epithelium and mesenchyme are two independent sources of WNT secretion (Farin et al., 2012; Gregorieff et al., 2005; Valenta et al., 2016). Paneth cells in the intestinal epithelium secrete WNT3, WNT6, and WNT9B; and myofibroblasts in the mesenchyme express WNT2, WNT4, and WNT5A (Gregorieff et al., 2005; Farin et al., 2012; Aoki et al., 2016; Stzepourginski et al., 2017; Valenta et al., 2016). Importantly, the epithelium and the mesenchyme are thought to be redundant sources of WNT secretion, with epithelial secreted WNT ligands being nonessential (Farin et al., 2012; Kabiri et al., 2014; San Roman et al., 2014; Valenta et al., 2016). When WNT3 or genes essential for WNT secretion (e.g., *Porcupine* and *Wntless*) were ablated in the intestinal epithelium, no apparent phenotype was observed (Farin et al., 2012). Knockouts (KOs) of genes specific to Paneth cells (e.g., *Atoh1* and *Gfi1*), the primary cellular source of epithelial WNT, also do not affect WNT pathway activation (Durand et al., 2012; Kim et al., 2012; Shroyer et al., 2005, 2007). These studies led to the prevailing notion that the epithelium is a redundant source of WNT and is not essential for CBC maintenance. By contrast, *in vitro*, mouse intestinal enteroids that contain only epithelial cells can be propagated without supplementing WNT ligands (Sato et al., 2009, 2011), suggesting that epithelial-secreted WNT is sufficient for stem cell proliferation. These discordant results warrant additional analyses on the role of epithelial-secreted WNT under nonhomeostatic situations.

We use rotavirus (RV) infection as an infection/injury model to test ISC responses to villus damage and whether mesenchymal or epithelial WNT plays a role in ISC activation. RV, a well-characterized, noninflammatory small intestinal viral pathogen, infects terminally differentiated mature cells, but not ISCs, in the small intestinal epithelium, resulting in watery diarrhea with vomiting, fever, and abdominal pain (Greenberg and Estes, 2009). RV infection alters the cytoskeleton and impairs host secretory pathways, leading to mislocalization of brush border enzymes and malabsorption, disruption of cell-cell junctions, increased permeability, cytotoxic effects, and activation of cell death (Ramig, 2004; Beau et al., 2007; Jourdan et al., 1998; Burns et al., 1995). Infection in adult mice is accompanied by a notable lack of villus blunting or epithelial ulceration, suggesting the induction of epithelial repair mechanisms that compensate and presumably replace the infected, lost cells (Ward et al., 1990; Burns et al., 1995; O'Neal et al., 1997; Blutt et al., 2012). Importantly, both the active and reserve ISC populations remain uninfected and undamaged during RV infection, providing an elegant model system to examine the ISC response within an intact stem cell compartment after injury. Our studies show that epithelial-derived signals regulate the hierarchical stem cell response when the niche remains intact and provide evidence for a functional role for epithelial WNT signaling.

RESULTS

RV Infection Does Not Infect the Crypt Compartment and Induces Crypt Expansion and Crypt-Villus Migration

Oral inoculation of adult mice with murine RV results in viral infection that is detected by viral shedding in stool (Figure 1A) (Ward et al., 1990; Burns et al., 1995; O'Neal et al., 1997; Blutt et al., 2012). Infected cells detected by anti-RV antibody were limited to the tips of the villi from 2 to 4 days post-infection (dpi) (Figures 1B and S1A). Maximum levels of viral shedding were observed 4 dpi (Figure 1A); therefore, all subsequent studies were performed at this time point. Importantly, the stem cell compartment is never infected (Figure 1B and S1A), and all cell types, including CBCs, reserve ISCs, and Paneth cells within the crypts, remained intact in RV-infected animals (Figures 1C, 3D, 3H, and S2).

To determine whether infected cells at the tip of the villus are damaged by infection, we examined cell morphology via H&E staining (Figure S1B), which showed increased cell shedding, nuclear mislocalization, and distorted and enlarged nuclei with

hypodense hematoxylin staining. Immunohistochemical staining of junctional protein E-cadherin showed its mislocalization from the cell membrane into the cytoplasm in addition to necrotic shedding cells (based on fragmented nuclei) (Figure S1C). To characterize the integrity of the brush border after infection, we evaluated villin, sodium-hydrogen antiporter 3 (NHE3), and ezrin, which are all normally located on the villus brush border (Figures S1D–S1F). On the infected villi, irregular and intensified villin staining was present on the apical cell surface with protein mislocalization into the cytoplasm (Figure S1D). NHE3 and ezrin protein staining was lost in parts of RV-infected villi (Figures S1E and S1F). To decipher the mechanism of cell death following infection, we probed for the anoikis marker phosphorylated myosin light chain (P-MLC) (Bullen et al., 2006) and the apoptosis marker cleaved caspase-3 (Figures S1G and S1H). We found that the number of P-MLC-labeled cells increased following infection but found few cleaved-caspase-3-labeled cells, suggesting that the majority of RV- infected cells undergo anoikis related cell death (Figures S1G and S1H).

To determine whether viral infection at the tip of the villi produced any response within the crypt region, we first examined proliferation of the crypts following RV infection. Expression of the proliferative marker PCNA indicated that crypts in RV-infected animals remained intact and that the $PCNA^+$ compartment was expanded (Figure 2A). Quantification of this expansion showed a 15-μm (or nearly one-third) increase in the height of $PCNA^+$ cells, with increased $PCNA^+$ cells per crypt following RV-infection (Figure 2B). The proliferative markers *Ki67* and *Pcna* were also transcriptionally upregulated in isolated crypts following infection (Figure 2C). Together, these experiments demonstrate an expanded and more proliferative $PCNA^+$ zone following RV infection.

Renewal of the intestinal epithelium depends on an upward migration of proliferating and differentiating cells from the crypt to the villus compartment. Previous studies have indicated that RV infection can affect cell migration in neonatal mice (Boshuizen et al., 2003; Preidis et al., 2012). Having documented that RV infection results in increased proliferation within the crypt region, we examined whether this expansion might impact upward migration of the differentiated progeny (Figure 2D). 2 hr after injecting the thymidine analog EdU, EdU^+ cells were restricted to the proliferating crypt zone in both control- and RV-infected animals (Figure 2D). 24 hr after EdU labeling, EdU^+ cells were observed to migrate out of the crypts and onto the villi (Figure 2D). Cell migration was assessed by measuring the absolute distance from the crypt-villus junction (just outside of the trans-amplifying zone) to the EdU^+ cell that had migrated the furthest. We determined the migration distance to be 22 μm, or 87%, faster in the RV-infected group than in the control group in 24 hr (Figures 2D and 2E, left). 48 hr after EdU injection, positive cells were already present at the tip of the villi in RV-infected mice, replacing RV-infected, damaged cells that had been shed lumenally, whereas EdU^+ cells were still migrating up the villi in control mice. (Figure 2D). Despite this more rapid cell migration up the villi, the total villus height was not different between RV- and control-infected animals, indicating that faster-migrating cells in RV-infected mice were replacing shed cells rather than extending the villus length (Figure 2E, right). These experiments demonstrate that RV infection stimulates a faster migration of proliferating cells from the crypt to the villi.

Active CBCs, but Not Alternative Reserve ISCs, Respond to RV Infection

In addition to the active CBC population, reserve ISCs have been postulated to exist within the small intestinal crypt (Potten, 1977; Potten and Hendry, 1975; Cheng and Leblond, 1974a; Henning and von Furstenberg, 2016; Mezoff and Shroyer, 2015; Beumer and Clevers, 2016). To determine whether a specific cell type responds to the injury from RV-induced damage, we evaluated the expression of putative ISC markers. Markers associated with CBCs alone (*Lgr5*, *Olfm4*, and *Ascl2*) (Barker et al., 2007; van der Flier et al., 2009a, 2009b) and with both CBCs and reserve ISCs (*Sox9* and *Lrig1*) (Van Landeghem et al., 2012; Powell et al., 2012) were significantly upregulated in crypts isolated from RV-infected mice, whereas markers associated with reserve ISC populations (*Bmi1*, *Hopx*, and *Dclk1*) (Yan et al., 2012; Takeda et al., 2011; Giannakis et al., 2006) showed minimal upregulation following infection (Figure 3A). These data suggest that the predominant response following RV infection occurs in the CBC population.

Given that some CBC markers would also be direct targets of the WNT and other signaling pathways, we tested whether transcriptional upregulation of CBC markers during RV infection indicates an increase in the CBC population. We utilized $Lgr5^{GFPCreERT}$ mice (Barker et al., 2007) in which LGR5-expressing cells are directly tagged with GFP (Figure 3B). A significant increase in the percentage of crypt cells expressing $LGR5^{GFP}$ and $LGR5^{GFP\text{-}high}$ was seen following infection by flow cytometry (Figures 3C and S3). Immunofluorescence staining indicated that LGR5-labeled CBCs were increased in number in crypts from RV-infected animals compared to control animals (Figure 3D). While the number of crypts per micrometer of intestine is unchanged (Figure S4C), an increase in LGR5-labeled crypts per micrometer of intestine was also observed when the entire small intestine was examined from infected mice (Figures S4A and S4B). It is possible that the increase in $LGR5^+$ crypts might be an artifact of the mosaic nature of the $Lgr5^{GFPCreERT}$ mice; however, assessment of OLFM4 (van der Flier et al., 2009a), another marker of CBCs, showed increased expression in crypts when comparing RV-infected and control animals (Figure 3E). Together, these data indicate an expansion of crypt-based columnar ISCs in response to RV infection.

To assess whether expansion of reserve ISCs also occurred in small intestinal crypts in response to RV infection, we first examined the reserve ISC marker BMI1. In $Bmi1^{CreERT};R26^{mTmG}$ mice (Yan et al., 2012), BMI1-labeled and reserve ISCs can be tagged with membrane-GFP following a dose of tamoxifen injection 1 day before harvest (Figure 3F). The $BMI1^+$ cell population remained very stable and comparable in control and RV-infected animals (Figures 3G and 3H). While *Bmi1* transcription was significantly upregulated with a small change (1.6-fold), a similar percentage of BMI1 cells in control- and RV-infected animals was observed by flow cytometry and immunofluorescence (Figures 3G and 3H). Lineage tracing also showed no change in BMI1 lineage following RV infection (Figure S5). Together, our data suggest that alternative reserve ISC populations do not

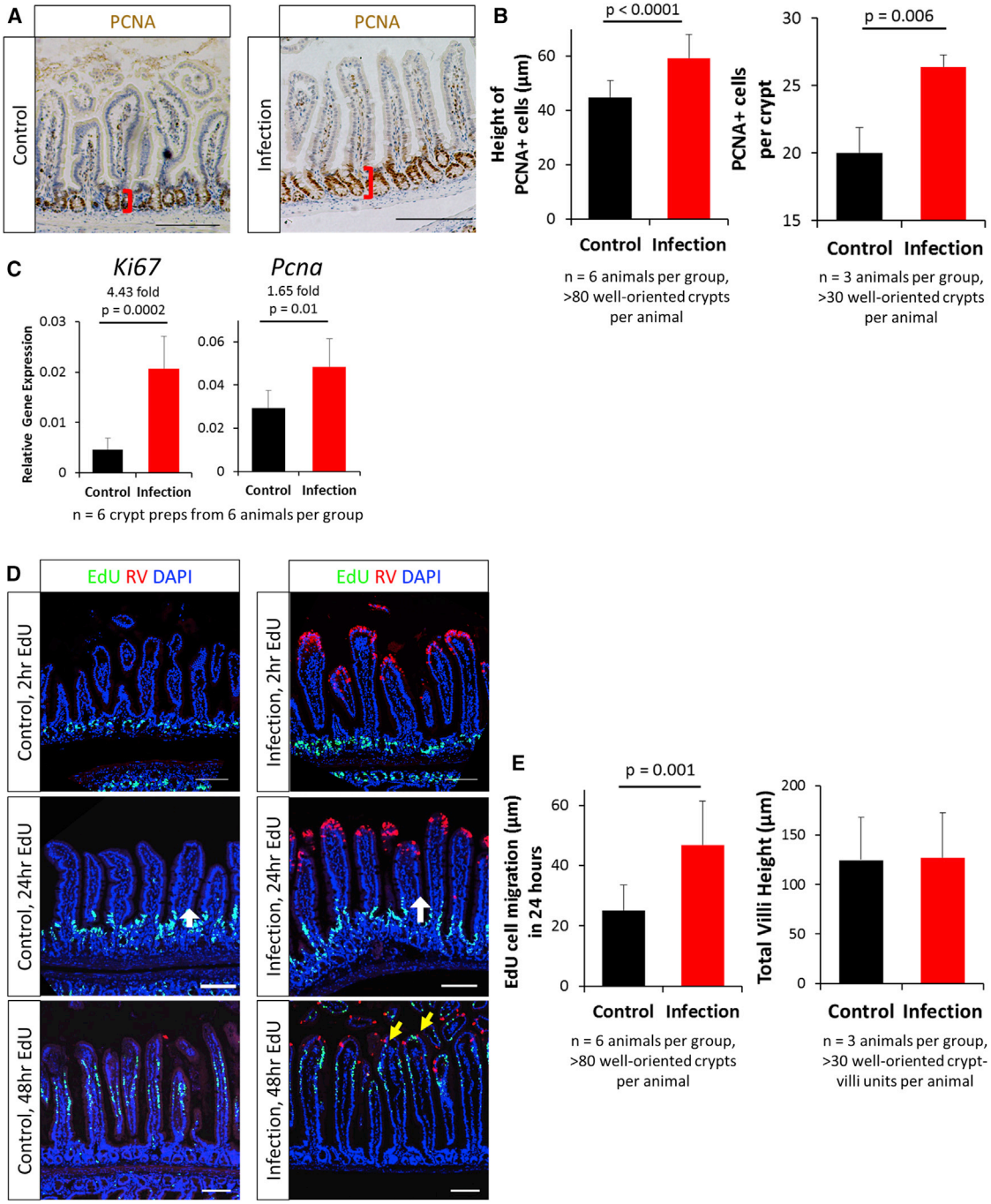

Figure 2. RV Infection Led to Increased Epithelial Proliferation and Increased Migration

(A) Representative immunohistochemistry images of PCNA$^+$ proliferating compartments. Red brackets represent the height of the PCNA$^+$ cells measured in (B).

(B) Quantification of height of PCNA$^+$ cells (left) and PCNA$^+$ cells per crypt (right).

(C) qRT-PCR results showing upregulation of the proliferative markers *Ki67* and *Pcna* in isolated epithelial crypts.

(D) Representative confocal images of cell migration in control- and RV-infected animals with 2-, 24-, and 48-hr EdU labeling. EdU$^+$ cells were restricted to the crypts after 2-hr EdU labeling. The length of 24-hr EdU migration was measured from the crypt-villi junction to the farthest EdU-labeled cells (white arrows). After 48 hr of labeling, EdU$^+$ cells were observed near RV-infected cells (yellow arrows).

(E) Quantification of cell migration 24 hr after EdU labeling (left) and total villi height (right). EdU cell migration distance is an absolute measure of distance from the crypt-villus junction (just outside of the transient amplifying [TA] zone) to the cell that had migrated the furthest.

Bars represent means ± SD. All statistical analyses were performed using Student's t test. Scale bars, 100 μm. See also Figures S3–S6.

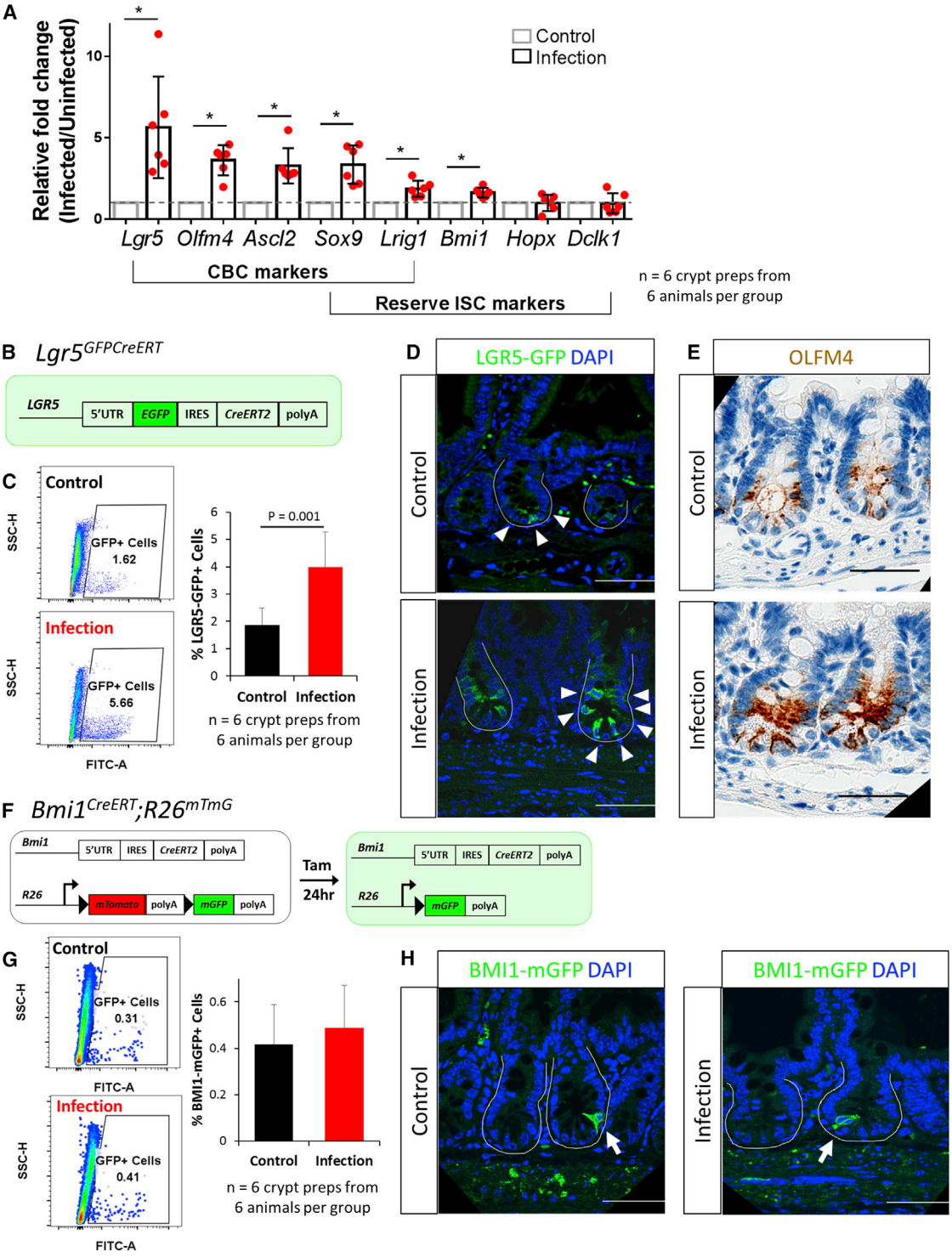

Figure 3. CBCs Are Induced following RV Infection

(A) qRT-PCR results showed upregulation of all CBC markers and some reserve ISC markers.

(B) Schematic of *Lgr5*^{GFPCreERT} mice. Cells expressing LGR5 are green.

(C) Representative flow cytometry analysis on control- and RV-infected *Lgr5*^{GFPCreERT}mice. Quantification of GFP^{+} cells using flow cytometry analysis on crypt-enriched epithelial preparations.

(D) Representative confocal images of *Lgr5*^{GFPCreERT} mice following control- and RV-infection. White arrowheads denote GFP^{+} cells.

(E) Representative light microscopy images of OLFM4 immunohistochemistry staining in control- and RV-infected animals.

(legend continued on next page)

respond to RV infection. These results demonstrate that, when intact, the CBC population remains the primary source of epithelial restitution and does not rely on alternative reserve ISC populations.

Epithelial WNT Secretion Is Essential for ISC Induction following RV Infection

The WNT signaling pathway is known to play a major role in stem cell proliferation and expansion (Fevr et al., 2007; Kuhnert et al., 2004; Pinto et al., 2003; Yan et al., 2017b). To determine whether RV infection induces WNT signaling, we examined the transcriptional profile of WNT ligands in isolated epithelial crypt and mesenchymal compartments of the small intestine (Gregorieff et al., 2005; Farin et al., 2012). Epithelial-expressed *Wnt3* and *Wnt9B* in crypt preparations were significantly upregulated in RV-infected mice compared with control mice (Figure 4A); however, the expression pattern of *Wnt3* in Paneth cells and other crypt cell types did not change when comparing control and RV-infected mice (Figure 4B). *Wnt2B*, *Wnt4*, and *Wnt5A* expression in mesenchymal preparations of infected mice were not affected (Figure 4A). Additionally, when we examined the WNT signaling amplifier R-spondin (R-spo) family members, we saw that *R-spo1* is upregulated in the mesenchymal preparations of infected mice (Figure S6). The expression of several well-established downstream WNT target genes (*Axin2, EphB2*, *Myc*, *Ccnd1*, *Cd44*, and *Tert*) was also upregulated in the crypts isolated from RV-infected animals (Figure 4C). RNA *in situ* hybridization confirmed WNT signaling upregulation by the expansion of *Axin2* expression in the crypts of the infected animals (Figure 4D). Immunofluorescence showed that expression of CD44v6, a pan crypt cell-surface marker that is regulated through the WNT pathway, was expressed on more crypt cells following infection (Figure 4E). Additionally, β-catenin, the intracellular transducer of the WNT signaling pathway, translocated from the cytoplasm to the nucleus in the crypts of RV-infected animals (Figure 4F). Collectively, these experiments show that RV-induced epithelial damage results in the increased transcriptional expression of epithelial WNT molecules, and they provide evidence of WNT signaling within the crypts.

Traditionally, the epithelium and the mesenchyme are thought to be redundant sources of WNT secretion during homeostasis, with the important WNT pathway signals derived from mesenchymal cells (Kabiri et al., 2014; Farin et al., 2012; Valenta et al., 2016; San Roman et al., 2014; de Groot et al., 2013). Whether there are unique functions of epithelial-secreted WNT ligands is currently unknown. The transcriptional upregulation of the epithelial-secreted WNT ligands *Wnt3* and *Wnt9B* (Figure 4A) suggested that epithelial WNTs might play an important role in the activation of LGR5$^+$ stem cells within the crypt following villus damage. To assess whether secretion of epithelial WNT was related to crypt expansion following infection, *Villin^{CreERT};WLS$^{f/f}$;R26^{mTmG}* (WLS KO) mice, in which WNT secretion in the epithelium is conditionally impaired, were infected with RV (Figures 5A and S7A) (Bänziger et al., 2006; Carpenter et al., 2010). Although RV infection induced upregulation of *Wnt5A* in mesenchymal preparations from WLS KO mice (Figure S7B), WNT pathway target genes were no longer upregulated in small intestinal crypts following infection (Figure 5B) compared to the upregulation seen in wild-type (WT) infected mice (Figure 4C). Further, CBC markers, including *Lgr5* and *Olfm4*, were not induced when epithelial WNT secretion was impaired (Figure 5C). The crypts were not expanded (Figures 5D and 5E), nor was there faster migration induced by infection, suggesting that epithelial WNT secretion plays an important role in these processes (Figures 5F and 5G). Additionally, while no overt phenotype was observed in the RV-infected WLS KO mice and RV shedding remained similar in the WT and WLS conditional KO model (Figure 5H), RV-infected cells in the WLS KO model were no longer localized to the tips of the villi (Figures 5F and S7A) compared to infected WT mice (Figures 1B and S1A). These findings indicate that epithelial-secreted WNT ligands are important for the regenerative crypt response following epithelial damage, and they may help restrict RV infection to the tip of the villi.

DISCUSSION

Understanding activation of stem cells within the niche environment is important for dissecting pathways that regulate epithelial repair. Intestinal regeneration after injury has been studied extensively using several models. For example, radiation-induced damage targets and kills LGR5$^+$ cycling CBCs. In this situation, the epithelium regenerates due to the plasticity of the reserve ISCs labeled by BMI1, HOPX, LRIG1, SOX9, and others, which repopulate the LGR5$^+$ cycling population within the base of the crypt (Hua et al., 2012; May et al., 2008; Metcalfe et al., 2014; Potten et al., 2009; Powell et al., 2012; Takeda et al., 2011; Yan et al., 2012; Yu, 2013). Chemotherapy treatments, such as doxorubicin, elicit injury patterns similar to radiation treatment, with loss of LGR5$^+$ populations within the crypt. Activation and increased proliferation of surface glycoprotein CD24-labeled ISCs following injury can reconstitute the damaged epithelium (Dekaney et al., 2009; Seiler et al., 2015). Genetic mouse models resulting in the direct ablation of LGR5-labeled CBCs have also shown the importance of the reserve ISCs as well as the newly characterized secretory and absorptive progenitors after LGR5$^+$ cell loss (Tetteh et al., 2016; van Es et al., 2012; Buczacki et al., 2013). Together, these studies suggest a plastic ISC environment in which many different stem cell types and progenitor cells can fulfill the demand of injury repair during CBC damage and loss. In the present work, we extend these studies by exploring how the crypt stem cell populations respond to villus-specific injury. RV infection has been linked to increased proliferation in the epithelium

(F) Schematic of *Bmi1^{CreERT};R26^{mTmG}* mice.
(G) Representative flow cytometry analysis on control- and RV-infected *Bmi1^{CreERT};R26^{mTmG}* mice. Quantification of BMI1-mGFP$^+$ cells using flow cytometry analysis on crypt-enriched epithelial preparations.
(H) Representative confocal images of BMI1-mGFP$^+$ mice following control- and RV-infection. White arrows denote BMI1-mGFP$^+$ cells.
Scale bars, 50 μm.

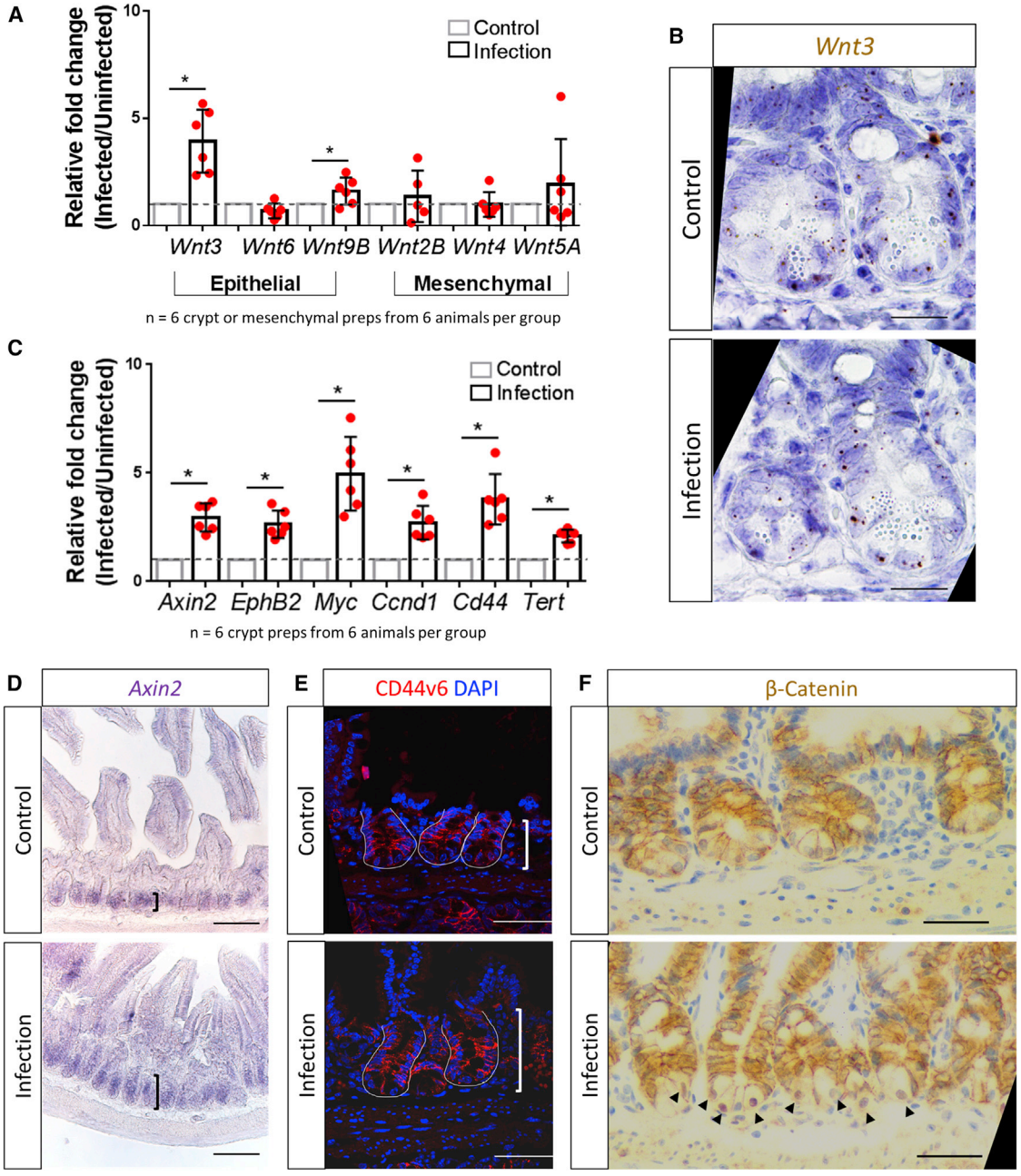

Figure 4. WNT Signaling Pathway Is Stimulated in Crypts following RV Infection

(A) qRT-PCR results showing upregulation of the epithelial-expressed *Wnt3* and *Wnt9B* in isolated epithelial crypt preparations. *Wnt2B*, *Wnt4*, and *Wnt5A* remained stable in mesenchymal preparations.

(B) RNAScope analysis showing *Wnt3* expression in Paneth cells and other crypt cell types in both control and RV infection.

(C) qRT-PCR results showing upregulation of well-established WNT signaling pathway target genes in isolated epithelial crypt preparations after RV infection.

(D) Representative RNA *in situ* hybridization images showed expansion of *Axin2* expression in RV infected animals.

(E) Representative immunofluorescence images showing that the WNT-target gene CD44v6 is expressed on more cells in the RV-infected animal.

(F) Representative immunohistochemistry staining of β-catenin, the intracellular transducer of the WNT signaling pathway. RV infection induces cytoplasm to nuclear translocation of β-catenin in the crypts (black arrowheads).

Scale bars represent 50 μm in (B), (E), and (F) and 100 μm in (D). See also Figure S6.

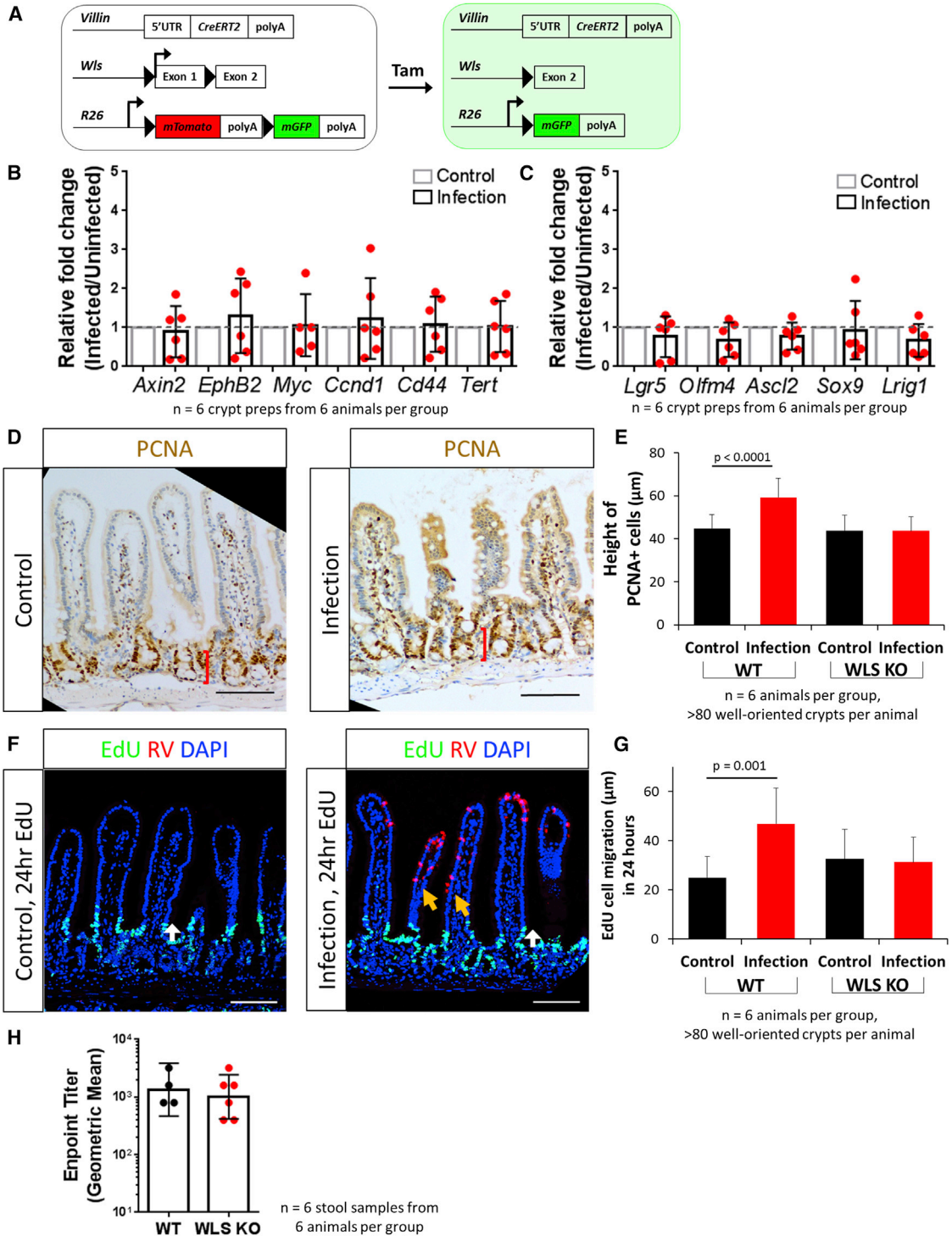

Figure 5. Epithelial-Secreted WNT Ligands Are Essential for RV-Induced Stem Cell Regeneration

(A) Schematic of *Villin*^{CreERT};*WLS*$^{f/f}$;*R26*^{mTmG} (WLS KO) mouse. Injections of tamoxifen allows for the conditional knockout of the *Wntless* gene in villin-expressing cells, impairing WNT secretion specifically in the epithelium.

(B) qRT-PCR results showed expression of WNT pathway target genes remain stable in isolated epithelial crypts following RV infection in WLS KO mice.

(C) qRT-PCR results showed expression of putative CBC markers remain stable in isolated epithelial crypts following RV infection in WLS KO mice.

(D) Representative immunohistochemistry staining of PCNA in control- and RV-infected WLS KO animals.

(E) Quantification of height of PCNA^{+} cell measurement in WT and WLS KO mice. Bars represent means ± SD.

(legend continued on next page)

(Boshuizen et al., 2003; Preidis et al., 2012). Our data demonstrate the LGR5$^+$ CBC population within the crypt environment is the one that expands during RV infection. In contrast to radiation, chemotherapy, and direct ablation, BMI1-marked cells do not respond to villus-specific damage (Figure 3). Because the crypt compartment is highly plastic, it is possible that BMI1-marked cells may have reverted back to the CBC state following RV infection, resulting in LGR5$^+$ cell expansion. However, this is unlikely, as we did not observe BMI1$^+$ cells at the CBC position (Figure 3), nor did we observe increased lineage tracing of BMI1$^+$ daughter cells following RV infection (Figure S5). Recent work suggests that BMI1$^+$ cells bear signatures of enteroendocrine cells, a differentiated, secretory cell type in the small intestine, making BMI1$^+$ cells a possible early progenitor committed to the enteroendocrine lineage (Jadhav et al., 2017; Yan et al., 2017a). Together, these results argue that RV-induced villus damage also does not affect the enteroendocrine progenitor population. These data build a more complex model of regeneration initiated in the stem cell niche in which LGR5$^+$ CBCs are important for homeostatic maintenance of the intestinal epithelium and are preferred to respond to villus epithelial damage by increasing proliferation and migration, while reserve ISCs and other progenitor cell types are only recruited during CBC loss and play an important role in regeneration of the crypt itself. Importantly, these data indicate there is a hierarchical control of the niche and the stem cells that comprise it.

WNT signaling is an important component of the ISC niche. Inhibition of global WNT secretion reduces proliferation and impairs epithelial homeostasis (Fevr et al., 2007; Kuhnert et al., 2004; Pinto et al., 2003; Valenta et al., 2016). While both the epithelium and mesenchyme secrete WNT molecules, epithelial-secreted WNT ligands are thought to be redundant and nonessential (Farin et al., 2012; Kabiri et al., 2014; San Roman et al., 2014; Valenta et al., 2016). When WNT3 and WNT secretion pathway genes (e.g., *Porcupine* and *Wntless*) were ablated in the intestinal epithelium, no apparent phenotype was observed (Farin et al., 2012). KOs of *Atoh1* and other genes specific to the Paneth cell, a known source of epithelial WNT secretion, also give no aberrant loss in WNT signaling activation (Durand et al., 2012; Kim et al., 2012). These findings have led to the hypothesis that mesenchymal WNT secretion is the primary mechanism for regulating the proliferative response in the stem cell niche. This idea is supported by several recent studies that have identified key mesenchymal cell types, marked by transcription factor *Foxl1* and surface antigen CD34, which can potentiate WNT signaling (Aoki et al., 2016; Stzepourginski et al., 2017). By contrast, our results show that epithelial-secreted WNT ligands are essential for the expansion of LGR5$^+$ cells and that proliferation and migration occur following virus-induced villus damage (Figures 3 and 4). Thus, although epithelial WNTs are thought to be nonessential for maintaining homeostasis, they are an important component of epithelial repair. It is important to note that our findings do not exclude the involvement of the mesenchyme. The upregulation of the WNT signaling amplifier *R-spo1* in the mesenchyme following infection raises the interesting possibility that epithelial WNT may be one arm of a broad inter-compartmental response to RV infection in which the induction of R-spo family proteins in the mesenchyme requires the priming by epithelial WNT to carry out injury repair after RV infection. This is in line with the recent publication on the nonequivalent yet cooperative role of R-spo and WNT on stem cell self-renewal (Yan et al., 2017b). Further, while RV-infected cells are restricted to the tip of the villi in WT mice, epithelial *Wntless* deletion resulted in an aberrant infection pattern in which infected cells can be observed midlength on the villi (Figure 5F). Since RV infects the terminally differentiated enterocytes that are present at the tips of the villi (Figures 1 and S1A) (Ward et al., 1990; Burns et al., 1995; O'Neal et al., 1997; Blutt et al., 2012), one possibility may be that the differentiation status of the enterocytes has been altered in the absence of epithelial-secreted WNT. Although previous studies did not find any significant differences in the differentiation pattern of epithelial-WNT impaired mice compared to WT mice (Kabiri et al., 2014; San Roman et al., 2014), it is possible that subtle cellular changes that are relevant to RV susceptibility and pathogenesis have occurred that were not detected in the initial comparison studies. Another explanation may be that epithelial WNT ligands, through their proliferative effects, affect the rate of cell migration and epithelial repair (Figures 2 and 5). Therefore, in the absence of epithelial WNT ligands, mature cells simply do not migrate as fast to the tip of the villi; thus, RV-infected cells are found in nontraditional locations. Future studies are needed to determine why RV-infected *Wntless* KO mice exhibit an altered infection pattern.

One of the key aspects to determining the mechanisms through which villus damage results in WNT secretion will be identifying which cell type is producing WNT following RV infection. A likely candidate is the Paneth cell, which has already been shown to secrete WNT (Sato et al., 2009, 2011). Our experiments, however, did not show changes in this cell type (Figure S2). Hence, there may exist an additional cell type with WNT-secreting ability that produces WNT only in the context of epithelial damage. Apoptotic cells during hydra head injury have been shown to be an unexpected source of WNT3 and are able to drive regeneration (Chera et al., 2009; Lengfeld et al., 2009). Similar mechanisms may exist in RV infection, where infected, apoptotic cells directly secrete WNT ligands, leading to increased stem cell proliferation within the crypt. Alternatively, other nonapoptotic damage signals produced by infected villus cells may indirectly stimulate WNT secretion from other cell types (e.g., Paneth cells), leading to stem cell activation. Such feedback mechanisms from differentiated cells to stem cells are not well understood in mammalian

(F) Representative image of EdU-labeled cell migration in control- and RV-infected animals in WLS KO mice. There was no induction of EdU$^+$ cell migration (white arrows). RV-infected cells were no longer restricted to the tip of the villi (orange arrows).
(G) Quantification of cell migration with 24 hr of EdU labeling in WT and WLS KO mice (white arrows in E). Bars represent means ± SD.
(H) Endpoint titer from stool ELISA of WT and WLS KO animals. Bars represent geometric mean ± 95% CI.
Scale bars, 100 μm. See also Figure S7.

systems, but several studies in the *Drosophila* gut have shown the importance of the JAK-STAT pathway (Beebe et al., 2010; Buchon et al., 2009; Jiang et al., 2016; Lin et al., 2010). Stress, injury, and bacterial infection can lead to cytokine production in damaged cells, stimulating the JAK-STAT pathway in WNT-producing cell types, which manifests into ultimate ISC proliferation (Jiang et al., 2016; Xu et al., 2011). Our previous study observed a robust upregulation of the interferon pathways in the intestinal epithelium following RV infection in the human intestinal enteroids (Saxena et al., 2017). Interferon production, with the subsequent activation of the JAK-STAT pathway, may serve as a bridge from infected cells to epithelial WNT production and CBC expansion (Saxena et al., 2017; Nava et al., 2010; Arnold et al., 2013). Future studies will focus on elucidating the cell type and mechanisms that elicit WNT signaling in response to RV infection.

Finally, while our data point to a necessary role in epithelial-secreted WNT ligands, we were not able to study whether epithelial-secreted WNT ligands are sufficient for the proliferative responses seen following RV infection. Future studies using the intestinal enteroid cultures that do not contain the mesenchyme will address the sufficiency of epithelial-signals in stem cell induction following infection. In addition, these cultures may facilitate the identification of additional epithelial sources of WNT ligands that are induced following infection. Alternatively, the mesenchyme may still potentiate regenerative responses in villus damage. Such close communication between epithelial and mesenchymal WNT signaling pathways has been shown in both the *Drosophila* midgut as well as mammalian small intestine (Kux and Pitsouli, 2014; Le Guen et al., 2015; Roulis and Flavell, 2016; Karlsson et al., 2000). Well-established feedback loops from Hedgehog and WNT signal pathways could serve as a potential link between the mesenchyme and the epithelium after RV infection (Büller et al., 2012; Kosinski et al., 2010). Several cell types recently identified to secrete R-spo and other growth factors in the mesenchyme could also serve as important catalysts for the WNT signaling pathway following epithelial injury (Stzepourginski et al., 2017; Aoki et al., 2016).

In summary, this study used RV infection as a model to study the injury-repair response from an intact ISC niche. We showed that LGR5$^+$ CBCs, when present, remain the primary source of epithelial restitution, and no other reserve cell types were needed for the response. In addition, epithelial-secreted WNT ligands are nonredundant, essential components of injury repair. These discoveries provide a framework for how cell types communicate in the intestinal tract and lay a foundation for developing regenerative treatments for intestinal injury.

EXPERIMENTAL PROCEDURES

Genetic Mouse Lines and Viral Infection

Lgr5^{GFPCreERT}, *R26*^{mTmG}, *Bmi1*^{CreERT}, and *Villin*^{CreERT} mice were obtained from The Jackson Laboratory (Bar Harbor, ME). *WLS*$^{f/f}$ mice were a generous gift from Dr. Jim Wells (Cincinnati Children's Hospital) (Carpenter et al., 2010). Mice aged 8–16 weeks (both males and females) were randomly assigned to control- or RV-infected groups with at least three mice per group per experiment. RV strain EC$_{WT}$ (P[17], G3) or PBS-control gut homogenate from previously infected mice was administered by oral gavage (O'Neal et al., 1997). All animals were housed in a physically separated BSL-2 animal facility. A 1×10^5 50% infectious dose (ID50) was used to obtain adequate infection (O'Neal et al., 1997). Fecal samples from each mouse were collected daily. Fecal ELISA was used to monitor RV infection as described previously (O'Neal et al., 1997). Mice were sacrificed 4 days following infection at the peak of viral shedding. To induce lineage tracing through *CreERT*, tamoxifen in 10% EtOH/corn oil was intraperitoneally injected. To label BMI1$^+$ cells and BMI1 lineage, 1 dose of 1 mg tamoxifen was injected in *Bmi1*^{CreERT};*R26*^{mTmG} mice 1 or 7 days before harvest, respectively. To conditionally knock out *Wntless*, 3 daily doses of 1 mg tamoxifen were injected in *Villin*^{CreERT};*WLS*$^{f/f}$;*R26*^{mTmG} mice 3 days before infection. To determine proliferation in the intestinal epithelium, 1 mg EdU in 10% DSMO/PBS was intraperitoneally injected at 2, 24, or 48 hr before harvest. All protocols were approved by the Baylor College of Medicine Institutional Animal Care and Use Committee (IACUC).

Crypt Purification and Mesenchymal Isolation

Intestinal crypts were prepared using previously described protocols, with modifications (Mahe et al., 2013; Gracz et al., 2012). Briefly, the entire small intestine was dissected out and flushed with ice-cold Ca^{2+}/$Mg2^+$-free Dulbecco's PBS (DPBS). Intestines were opened lengthwise and cut into 1-cm pieces. Tissues were incubated with chelating buffer (2 mM EDTA in DPBS) on ice for 30 min by gentle shaking. Chelating buffer was then replaced with shaking buffer (1% [43.3 mM] sucrose, 1% [54.9 mM] sorbitol in DPBS) and manually shaken for ~1–2 min to disassociate crypts. Intestinal crypts were filtered through a 70-μm cell strainer (BD Falcon) and then spun down at 150 × *g*, 4°C for 5 min. Remaining tissue after epithelial purification was harvested as mesenchyme.

Statistical Analysis

Data are presented as means ± SD. The n in all experiments refers to biological replicates (different animals) in each group. n for each experiment is listed in each figure. Statistical comparisons between two groups were analyzed using the Student's t test. Significance was taken as $p < 0.05$. All analyses were performed using GraphPad Prism version 5.01 (GraphPad Software, La Jolla, CA).

DATA AND SOFTWARE AVAILABILITY

The accession numbers for the flow cytometry data reported in this paper are Flow Repository: FR-FCM-ZYF8 and FR-FCM-ZYF9.

SUPPLEMENTAL INFORMATION

Supplemental Information includes Supplemental Experimental Procedures, seven figures, and two tables and can be found with this article online at https://doi.org/10.1016/j.celrep.2017.12.093.

ACKNOWLEDGMENTS

We thank Susan Henning for insightful consultation throughout the project and the members of the Estes, Donowitz, and Shroyer labs for critical input on experiments and data analysis. We thank Joel Sederstrom, Dr. Fabio Stossi, Dr. Milton Finegold, and Dr. Patricia Castro for their expert assistance. This work was performed as part of the Intestinal Stem Cell Consortium with funding from the NIH through grants U01 DK103168, U01 DK103168-03S1, and U01 DK103168-02S1 to M.K.E. and grant F30 DK107173 to W.Y.Z. This project was also supported by the Cellular and Molecular Morphology Core of the Texas Medical Center Digestive Disease Center (funded by NIH grant P30DK056338) and the Advanced Technology Core Laboratories at Baylor College of Medicine, including the Cytometry and Cell Sorting Core (funded by NIH NIAID grant P30AI036211, NCI grant P30CA125123, and NCRR grant S10RR024574), the Pathology and Histology Core (funded by NCI grant P30CA125123), and the Integrated Microscopy Core (funded by NIH grants DK56338 and CA125123, CPRIT grant RP150578, the Dan L. Duncan Comprehensive Cancer Center [P30CA125123], and the John S. Dunn Gulf Coast Consortium for Chemical Genomics [CPRIT RP150578]).

AUTHOR CONTRIBUTIONS

S.E.B. and M.K.E. conceptualized the study. M.K.E., S.E.B., and N.F.S. supervised all studies performed. W.Y.Z., M.-S.C., X.-L.Z., and D.C.-A. designed and performed experiments. W.Y.Z., Y.-H.L, S.E.B., N.F.S., and O.D.K. critically analyzed experimental data. W.Y.Z. wrote the manuscript. S.E.B., N.F.S., M.K.E., and M.D. provided critical input in manuscript revision. All authors contributed to the writing or editing of the final manuscript.

DECLARATION OF INTERESTS

The authors declare no competing interests.

Received: July 25, 2017
Revised: November 16, 2017
Accepted: December 24, 2017
Published: January 23, 2018

REFERENCES

Aoki, R., Shoshkes-Carmel, M., Gao, N., Shin, S., May, C.L., Golson, M.L., Zahm, A.M., Ray, M., Wiser, C.L., Wright, C.V., and Kaestner, K.H. (2016). Foxl1-expressing mesenchymal cells constitute the intestinal stem cell niche. Cell. Mol. Gastroenterol. Hepatol. *2*, 175–188.

Arnold, M.M., Sen, A., Greenberg, H.B., and Patton, J.T. (2013). The battle between rotavirus and its host for control of the interferon signaling pathway. PLoS Pathog. *9*, e1003064.

Bänziger, C., Soldini, D., Schütt, C., Zipperlen, P., Hausmann, G., and Basler, K. (2006). Wntless, a conserved membrane protein dedicated to the secretion of Wnt proteins from signaling cells. Cell *125*, 509–522.

Barker, N., van Es, J.H., Kuipers, J., Kujala, P., van den Born, M., Cozijnsen, M., Haegebarth, A., Korving, J., Begthel, H., Peters, P.J., and Clevers, H. (2007). Identification of stem cells in small intestine and colon by marker gene Lgr5. Nature *449*, 1003–1007.

Beau, I., Berger, A., and Servin, A.L. (2007). Rotavirus impairs the biosynthesis of brush-border-associated dipeptidyl peptidase IV in human enterocyte-like Caco-2/TC7 cells. Cell. Microbiol. *9*, 779–789.

Beebe, K., Lee, W.C., and Micchelli, C.A. (2010). JAK/STAT signaling coordinates stem cell proliferation and multilineage differentiation in the Drosophila intestinal stem cell lineage. Dev. Biol. *338*, 28–37.

Beumer, J., and Clevers, H. (2016). Regulation and plasticity of intestinal stem cells during homeostasis and regeneration. Development *143*, 3639–3649.

Blutt, S.E., Miller, A.D., Salmon, S.L., Metzger, D.W., and Conner, M.E. (2012). IgA is important for clearance and critical for protection from rotavirus infection. Mucosal Immunol. *5*, 712–719.

Boshuizen, J.A., Reimerink, J.H., Korteland-van Male, A.M., van Ham, V.J., Koopmans, M.P., Büller, H.A., Dekker, J., and Einerhand, A.W. (2003). Changes in small intestinal homeostasis, morphology, and gene expression during rotavirus infection of infant mice. J. Virol. *77*, 13005–13016.

Buchon, N., Broderick, N.A., Poidevin, M., Pradervand, S., and Lemaitre, B. (2009). Drosophila intestinal response to bacterial infection: activation of host defense and stem cell proliferation. Cell Host Microbe *5*, 200–211.

Buczacki, S.J., Zecchini, H.I., Nicholson, A.M., Russell, R., Vermeulen, L., Kemp, R., and Winton, D.J. (2013). Intestinal label-retaining cells are secretory precursors expressing Lgr5. Nature *495*, 65–69.

Bullen, T.F., Forrest, S., Campbell, F., Dodson, A.R., Hershman, M.J., Pritchard, D.M., Turner, J.R., Montrose, M.H., and Watson, A.J. (2006). Characterization of epithelial cell shedding from human small intestine. Lab. Invest. *86*, 1052–1063.

Büller, N.V., Rosekrans, S.L., Westerlund, J., and van den Brink, G.R. (2012). Hedgehog signaling and maintenance of homeostasis in the intestinal epithelium. Physiology (Bethesda) *27*, 148–155.

Burns, J.W., Krishnaney, A.A., Vo, P.T., Rouse, R.V., Anderson, L.J., and Greenberg, H.B. (1995). Analyses of homologous rotavirus infection in the mouse model. Virology *207*, 143–153.

Carpenter, A.C., Rao, S., Wells, J.M., Campbell, K., and Lang, R.A. (2010). Generation of mice with a conditional null allele for Wntless. Genesis *48*, 554–558.

Cheng, H., and Leblond, C.P. (1974a). Origin, differentiation and renewal of the four main epithelial cell types in the mouse small intestine. I. Columnar cell. Am. J. Anat. *141*, 461–479.

Cheng, H., and Leblond, C.P. (1974b). Origin, differentiation and renewal of the four main epithelial cell types in the mouse small intestine. V. Unitarian Theory of the origin of the four epithelial cell types. Am. J. Anat. *141*, 537–561.

Chera, S., Ghila, L., Dobretz, K., Wenger, Y., Bauer, C., Buzgariu, W., Martinou, J.C., and Galliot, B. (2009). Apoptotic cells provide an unexpected source of Wnt3 signaling to drive hydra head regeneration. Dev. Cell *17*, 279–289.

Clevers, H., and Nusse, R. (2012). Wnt/β-catenin signaling and disease. Cell *149*, 1192–1205.

Clevers, H., Loh, K.M., and Nusse, R. (2014). Stem cell signaling. An integral program for tissue renewal and regeneration: Wnt signaling and stem cell control. Science *346*, 1248012.

de Groot, R.E., Farin, H.F., Macůrková, M., van Es, J.H., Clevers, H.C., and Korswagen, H.C. (2013). Retromer dependent recycling of the Wnt secretion factor Wls is dispensable for stem cell maintenance in the mammalian intestinal epithelium. PLoS ONE *8*, e76971.

Dekaney, C.M., Gulati, A.S., Garrison, A.P., Helmrath, M.A., and Henning, S.J. (2009). Regeneration of intestinal stem/progenitor cells following doxorubicin treatment of mice. Am. J. Physiol. Gastrointest. Liver Physiol. *297*, G461–G470.

Durand, A., Donahue, B., Peignon, G., Letourneur, F., Cagnard, N., Slomianny, C., Perret, C., Shroyer, N.F., and Romagnolo, B. (2012). Functional intestinal stem cells after Paneth cell ablation induced by the loss of transcription factor Math1 (Atoh1). Proc. Natl. Acad. Sci. USA *109*, 8965–8970.

Farin, H.F., Van Es, J.H., and Clevers, H. (2012). Redundant sources of Wnt regulate intestinal stem cells and promote formation of Paneth cells. Gastroenterology *143*, 1518–1529.e7.

Fevr, T., Robine, S., Louvard, D., and Huelsken, J. (2007). Wnt/beta-catenin is essential for intestinal homeostasis and maintenance of intestinal stem cells. Mol. Cell. Biol. *27*, 7551–7559.

Giannakis, M., Stappenbeck, T.S., Mills, J.C., Leip, D.G., Lovett, M., Clifton, S.W., Ippolito, J.E., Glasscock, J.I., Arumugam, M., Brent, M.R., and Gordon, J.I. (2006). Molecular properties of adult mouse gastric and intestinal epithelial progenitors in their niches. J. Biol. Chem. *281*, 11292–11300.

Gracz, A., Puthoff, B., and Magness, S.T. (2012). Identification, isolation, and culture of intestinal epithelial stem cells from murine intestine. Methods Mol. Biol. *879*, 89–107.

Greenberg, H.B., and Estes, M.K. (2009). Rotaviruses: from pathogenesis to vaccination. Gastroenterology *136*, 1939–1951.

Gregorieff, A., Pinto, D., Begthel, H., Destrée, O., Kielman, M., and Clevers, H. (2005). Expression pattern of Wnt signaling components in the adult intestine. Gastroenterology *129*, 626–638.

Henning, S.J., and von Furstenberg, R.J. (2016). GI stem cells - new insights into roles in physiology and pathophysiology. J. Physiol. *594*, 4769–4779.

Hua, G., Thin, T.H., Feldman, R., Haimovitz-Friedman, A., Clevers, H., Fuks, Z., and Kolesnick, R. (2012). Crypt base columnar stem cells in small intestines of mice are radioresistant. Gastroenterology *143*, 1266–1276.

Jadhav, U., Saxena, M., O'Neill, N.K., Saadatpour, A., Yuan, G.-C., Herbert, Z., Murata, K., and Shivdasani, R.A. (2017). Dynamic reorganization of chromatin accessibility signatures during dedifferentiation of secretory precursors into Lgr5+ intestinal stem cells. Cell Stem Cell *21*, 65–77.e5.

Jiang, H., Tian, A., and Jiang, J. (2016). Intestinal stem cell response to injury: lessons from Drosophila. Cell. Mol. Life Sci. *73*, 3337–3349.

Jourdan, N., Brunet, J.P., Sapin, C., Blais, A., Cotte-Laffitte, J., Forestier, F., Quero, A.M., Trugnan, G., and Servin, A.L. (1998). Rotavirus infection reduces sucrase-isomaltase expression in human intestinal epithelial cells by perturbing protein targeting and organization of microvillar cytoskeleton. J. Virol. *72*, 7228–7236.

Kabiri, Z., Greicius, G., Madan, B., Biechele, S., Zhong, Z., Zaribafzadeh, H., Edison, Aliyev, J., Wu, Y., Bunte, R., et al. (2014). Stroma provides an intestinal stem cell niche in the absence of epithelial Wnts. Development *141*, 2206–2215.

Karlsson, L., Lindahl, P., Heath, J.K., and Betsholtz, C. (2000). Abnormal gastrointestinal development in PDGF-A and PDGFR-(alpha) deficient mice implicates a novel mesenchymal structure with putative instructive properties in villus morphogenesis. Development *127*, 3457–3466.

Kim, T.H., Escudero, S., and Shivdasani, R.A. (2012). Intact function of Lgr5 receptor-expressing intestinal stem cells in the absence of Paneth cells. Proc. Natl. Acad. Sci. USA *109*, 3932–3937.

Kosinski, C., Stange, D.E., Xu, C., Chan, A.S., Ho, C., Yuen, S.T., Mifflin, R.C., Powell, D.W., Clevers, H., Leung, S.Y., and Chen, X. (2010). Indian hedgehog regulates intestinal stem cell fate through epithelial-mesenchymal interactions during development. Gastroenterology *139*, 893–903.

Kühl, S.J., and Kühl, M. (2013). On the role of Wnt/β-catenin signaling in stem cells. Biochim. Biophys. Acta *1830*, 2297–2306.

Kuhnert, F., Davis, C.R., Wang, H.T., Chu, P., Lee, M., Yuan, J., Nusse, R., and Kuo, C.J. (2004). Essential requirement for Wnt signaling in proliferation of adult small intestine and colon revealed by adenoviral expression of Dickkopf-1. Proc. Natl. Acad. Sci. USA *101*, 266–271.

Kux, K., and Pitsouli, C. (2014). Tissue communication in regenerative inflammatory signaling: lessons from the fly gut. Front. Cell. Infect. Microbiol. *4*, 49.

Le Guen, L., Marchal, S., Faure, S., and de Santa Barbara, P. (2015). Mesenchymal-epithelial interactions during digestive tract development and epithelial stem cell regeneration. Cell. Mol. Life Sci. *72*, 3883–3896.

Lengfeld, T., Watanabe, H., Simakov, O., Lindgens, D., Gee, L., Law, L., Schmidt, H.A., Ozbek, S., Bode, H., and Holstein, T.W. (2009). Multiple Wnts are involved in Hydra organizer formation and regeneration. Dev. Biol. *330*, 186–199.

Lin, G., Xu, N., and Xi, R. (2010). Paracrine unpaired signaling through the JAK/STAT pathway controls self-renewal and lineage differentiation of Drosophila intestinal stem cells. J. Mol. Cell Biol. *2*, 37–49.

Mahe, M.M., Aihara, E., Schumacher, M.A., Zavros, Y., Montrose, M.H., Helmrath, M.A., Sato, T., and Shroyer, N.F. (2013). Establishment of gastrointestinal epithelial organoids. Curr. Protoc. Mouse Biol. *3*, 217–240.

May, R., Riehl, T.E., Hunt, C., Sureban, S.M., Anant, S., and Houchen, C.W. (2008). Identification of a novel putative gastrointestinal stem cell and adenoma stem cell marker, doublecortin and CaM kinase-like-1, following radiation injury and in adenomatous polyposis coli/multiple intestinal neoplasia mice. Stem Cells *26*, 630–637.

Metcalfe, C., Kljavin, N.M., Ybarra, R., and de Sauvage, F.J. (2014). Lgr5+ stem cells are indispensable for radiation-induced intestinal regeneration. Cell Stem Cell *14*, 149–159.

Mezoff, E., and Shroyer, N. (2015). Anatomy and physiology of the small and large intestines. In Pediatric Gastrointestinal and Liver Disease, Fifth Edition, R. Wyllie, J.S. Hyams, and M. Kay, eds. (Elsevier), pp. 345–359.

Nava, P., Koch, S., Laukoetter, M.G., Lee, W.Y., Kolegraff, K., Capaldo, C.T., Beeman, N., Addis, C., Gerner-Smidt, K., Neumaier, I., et al. (2010). Interferon-γ regulates intestinal epithelial homeostasis through converging β-catenin signaling pathways. Immunity *32*, 392–402.

Nusse, R., and Varmus, H. (2012). Three decades of Wnts: a personal perspective on how a scientific field developed. EMBO J. *31*, 2670–2684.

O'Neal, C.M., Crawford, S.E., Estes, M.K., and Conner, M.E. (1997). Rotavirus virus-like particles administered mucosally induce protective immunity. J. Virol. *71*, 8707–8717.

Pinto, D., Gregorieff, A., Begthel, H., and Clevers, H. (2003). Canonical Wnt signals are essential for homeostasis of the intestinal epithelium. Genes Dev. *17*, 1709–1713.

Potten, C.S. (1977). Extreme sensitivity of some intestinal crypt cells to X and gamma irradiation. Nature *269*, 518–521.

Potten, C.S. (1997). Epithelial cell growth and differentiation. II. Intestinal apoptosis. Am. J. Physiol. *273*, G253–G257.

Potten, C.S., and Hendry, J.H. (1975). Differential regeneration of intestinal proliferative cells and cryptogenic cells after irradiation. Int. J. Radiat. Biol. Relat. Stud. Phys. Chem. Med. *27*, 413–424.

Potten, C.S., Gandara, R., Mahida, Y.R., Loeffler, M., and Wright, N.A. (2009). The stem cells of small intestinal crypts: where are they? Cell Prolif. *42*, 731–750.

Poulin, E.J., Powell, A.E., Wang, Y., Li, Y., Franklin, J.L., and Coffey, R.J. (2014). Using a new Lrig1 reporter mouse to assess differences between two Lrig1 antibodies in the intestine. Stem Cell Res. (Amst.) *13* (*3 Pt A*), 422–430.

Powell, A.E., Wang, Y., Li, Y., Poulin, E.J., Means, A.L., Washington, M.K., Higginbotham, J.N., Juchheim, A., Prasad, N., Levy, S.E., et al. (2012). The pan-ErbB negative regulator Lrig1 is an intestinal stem cell marker that functions as a tumor suppressor. Cell *149*, 146–158.

Preidis, G.A., Saulnier, D.M., Blutt, S.E., Mistretta, T.A., Riehle, K.P., Major, A.M., Venable, S.F., Barrish, J.P., Finegold, M.J., Petrosino, J.F., et al. (2012). Host response to probiotics determined by nutritional status of rotavirus-infected neonatal mice. J. Pediatr. Gastroenterol. Nutr. *55*, 299–307.

Ramig, R.F. (2004). Pathogenesis of intestinal and systemic rotavirus infection. J. Virol. *78*, 10213–10220.

Roche, K.C., Gracz, A.D., Liu, X.F., Newton, V., Akiyama, H., and Magness, S.T. (2015). SOX9 maintains reserve stem cells and preserves radioresistance in mouse small intestine. Gastroenterology *149*, 1553–1563.e10.

Roulis, M., and Flavell, R.A. (2016). Fibroblasts and myofibroblasts of the intestinal lamina propria in physiology and disease. Differentiation *92*, 116–131.

San Roman, A.K., Jayewickreme, C.D., Murtaugh, L.C., and Shivdasani, R.A. (2014). Wnt secretion from epithelial cells and subepithelial myofibroblasts is not required in the mouse intestinal stem cell niche in vivo. Stem Cell Reports *2*, 127–134.

Sato, T., Vries, R.G., Snippert, H.J., van de Wetering, M., Barker, N., Stange, D.E., van Es, J.H., Abo, A., Kujala, P., Peters, P.J., and Clevers, H. (2009). Single Lgr5 stem cells build crypt-villus structures in vitro without a mesenchymal niche. Nature *459*, 262–265.

Sato, T., van Es, J.H., Snippert, H.J., Stange, D.E., Vries, R.G., van den Born, M., Barker, N., Shroyer, N.F., van de Wetering, M., and Clevers, H. (2011). Paneth cells constitute the niche for Lgr5 stem cells in intestinal crypts. Nature *469*, 415–418.

Saxena, K., Simon, L.M., Zeng, X.L., Blutt, S.E., Crawford, S.E., Sastri, N.P., Karandikar, U.C., Ajami, N.J., Zachos, N.C., Kovbasnjuk, O., et al. (2017). A paradox of transcriptional and functional innate interferon responses of human intestinal enteroids to enteric virus infection. Proc. Natl. Acad. Sci. USA *114*, E570–E579.

Seiler, K.M., Schenhals, E.L., von Furstenberg, R.J., Allena, B.K., Smith, B.J., Scaria, D., Bresler, M.N., Dekaney, C.M., and Henning, S.J. (2015). Tissue underlying the intestinal epithelium elicits proliferation of intestinal stem cells following cytotoxic damage. Cell Tissue Res. *361*, 427–438.

Shroyer, N.F., Wallis, D., Venken, K.J., Bellen, H.J., and Zoghbi, H.Y. (2005). Gfi1 functions downstream of Math1 to control intestinal secretory cell subtype allocation and differentiation. Genes Dev. *19*, 2412–2417.

Shroyer, N.F., Helmrath, M.A., Wang, V.Y.C., Antalffy, B., Henning, S.J., and Zoghbi, H.Y. (2007). Intestine-specific ablation of mouse atonal homolog 1 (Math1) reveals a role in cellular homeostasis. Gastroenterology *132*, 2478–2488.

Shroyer, N.F., Bell, K., and Lo, Y.-H. (2015). Biology of intestinal epithelial stem cells. In Intestinal Tumorigenesis: Mechanisms of Development & Progression, V.W. Yang and A.B. Bialkowska, eds. (Springer International Publishing), pp. 55–99.

Stzepourginski, I., Nigro, G., Jacob, J.M., Dulauroy, S., Sansonetti, P.J., Eberl, G., and Peduto, L. (2017). CD34+ mesenchymal cells are a major component of the intestinal stem cells niche at homeostasis and after injury. Proc. Natl. Acad. Sci. USA *114*, E506–E513.

Takeda, N., Jain, R., LeBoeuf, M.R., Wang, Q., Lu, M.M., and Epstein, J.A. (2011). Interconversion between intestinal stem cell populations in distinct niches. Science *334*, 1420–1424.

Tetteh, P.W., Basak, O., Farin, H.F., Wiebrands, K., Kretzschmar, K., Begthel, H., van den Born, M., Korving, J., de Sauvage, F., van Es, J.H., et al. (2016). Replacement of lost Lgr5-positive stem cells through plasticity of their enterocyte-lineage daughters. Cell Stem Cell *18*, 203–213.

Tian, H., Biehs, B., Warming, S., Leong, K.G., Rangell, L., Klein, O.D., and de Sauvage, F.J. (2011). A reserve stem cell population in small intestine renders Lgr5-positive cells dispensable. Nature *478*, 255–259.

Valenta, T., Degirmenci, B., Moor, A.E., Herr, P., Zimmerli, D., Moor, M.B., Hausmann, G., Cantù, C., Aguet, M., and Basler, K. (2016). Wnt ligands secreted by subepithelial mesenchymal cells are essential for the survival of intestinal stem cells and gut homeostasis. Cell Rep. *15*, 911–918.

van der Flier, L.G., and Clevers, H. (2009). Stem cells, self-renewal, and differentiation in the intestinal epithelium. Annu. Rev. Physiol. *71*, 241–260.

van der Flier, L.G., Haegebarth, A., Stange, D.E., van de Wetering, M., and Clevers, H. (2009a). OLFM4 is a robust marker for stem cells in human intestine and marks a subset of colorectal cancer cells. Gastroenterology *137*, 15–17.

van der Flier, L.G., van Gijn, M.E., Hatzis, P., Kujala, P., Haegebarth, A., Stange, D.E., Begthel, H., van den Born, M., Guryev, V., Oving, I., et al. (2009b). Transcription factor achaete scute-like 2 controls intestinal stem cell fate. Cell *136*, 903–912.

van Es, J.H., Sato, T., van de Wetering, M., Lyubimova, A., Yee Nee, A.N., Gregorieff, A., Sasaki, N., Zeinstra, L., van den Born, M., Korving, J., et al. (2012). Dll1+ secretory progenitor cells revert to stem cells upon crypt damage. Nat. Cell Biol. *14*, 1099–1104.

Van Landeghem, L., Santoro, M.A., Krebs, A.E., Mah, A.T., Dehmer, J.J., Gracz, A.D., Scull, B.P., McNaughton, K., Magness, S.T., and Lund, P.K. (2012). Activation of two distinct Sox9-EGFP-expressing intestinal stem cell populations during crypt regeneration after irradiation. Am. J. Physiol. Gastrointest. Liver Physiol. *302*, G1111–G1132.

Ward, R.L., McNeal, M.M., and Sheridan, J.F. (1990). Development of an adult mouse model for studies on protection against rotavirus. J. Virol. *64*, 5070–5075.

Xu, N., Wang, S.Q., Tan, D., Gao, Y., Lin, G., and Xi, R. (2011). EGFR, Wingless and JAK/STAT signaling cooperatively maintain Drosophila intestinal stem cells. Dev. Biol. *354*, 31–43.

Yan, K.S., Chia, L.A., Li, X., Ootani, A., Su, J., Lee, J.Y., Su, N., Luo, Y., Heilshorn, S.C., Amieva, M.R., et al. (2012). The intestinal stem cell markers Bmi1 and Lgr5 identify two functionally distinct populations. Proc. Natl. Acad. Sci. USA *109*, 466–471.

Yan, K.S., Gevaert, O., Zheng, G.X.Y., Anchang, B., Probert, C.S., Larkin, K.A., Davies, P.S., Cheng, Z.F., Kaddis, J.S., Han, A., et al. (2017a). Intestinal enteroendocrine lineage cells possess homeostatic and injury-inducible stem cell activity. Cell Stem Cell *21*, 78–90.e6.

Yan, K.S., Janda, C.Y., Chang, J., Zheng, G.X.Y., Larkin, K.A., Luca, V.C., Chia, L.A., Mah, A.T., Han, A., Terry, J.M., et al. (2017b). Non-equivalence of Wnt and R-spondin ligands during Lgr5+ intestinal stem-cell self-renewal. Nature *545*, 238–242.

Yu, J. (2013). Intestinal stem cell injury and protection during cancer therapy. Transl. Cancer Res. *2*, 384–396.

Cell Reports, Volume *22*

Supplemental Information

Epithelial WNT Ligands Are Essential Drivers of Intestinal Stem Cell Activation

Winnie Y. Zou, Sarah E. Blutt, Xi-Lei Zeng, Min-Shan Chen, Yuan-Hung Lo, David Castillo-Azofeifa, Ophir D. Klein, Noah F. Shroyer, Mark Donowitz, and Mary K. Estes

SUPPLEMENTAL EXPERIMENTAL PROCEDURES

Flow cytometry. Crypts isolated from previous steps were made into single cell suspensions by incubating with 0.8mg/mL dispase solution at 37°C for 10min. Solution was vortexed every 2min to ensure single cell dissociation. 1mL Fetal Bovine Serum (FBS) was added to stop the enzymatic digestion and 50uL 10mg/µL DNAse was added to prevent cell clumps. Single cells were filtered through a 40µm cell strainer (BD Falcon) and then spun down at 1000g, 4°C for 5 min. 10% FBS in HBSS was used to wash cells before proceeding to antibody staining. Please refer to **Table S1** for a list of antibodies and respective dilutions. n in all experiments refer to separate crypt preps from different animals in each group. Discrimination of each cell population via flow cytometry is shown in **Figure S3**. Dead cells and doublets were excluded using side and forward scatters. At least 30,000 live, epithelial cells were collected using the $EpCam^{APC}$/DAPI gate for analysis. Lgr5-GFP^{high} population was analyzed using previously published gating schemes (Sato et al., 2009). All data were collected using BD LSRFortessa™ and analyzed on FlowJo software. Flow cytometry data were uploaded to Flow Repository with IDs: FR-FCM-ZYF8 and FR-FCM-ZYF9.

Reverse transcription-quantitative PCR (RT-qPCR) analysis. Crypts were isolated from control- or RV-infected mice small intestine. Total RNA was extracted from isolated crypts using the Zymo Research Directo-zol™ RNA kit, following the manufacture's protocol. The amount and purity of RNA were determined using a NanoDrop spectrophotometer (Thermo Scientific, Waltham, TA). Reverse transcription-quantitative PCR (RT-qPCR) was performed on a StepOnePlus real-time PCR system (Applied Biosystems, Foster City, CA), using One-Step RT-qPCR ToughMix with the ROX reference dye according to the manufacturer's protocol (Quanta Biosciences, Gaithersburg,

MD). TaqMan primer-probe mixes were obtained from Molecular Probes (Eugene, OR), with the assay identification numbers listed in **Table S2**. Expression levels were normalized to *Gapdh* levels and analyzed with StepOne v2.1 software (Applied Biosystems) by using the 2−ΔΔCT method as previously described (Schmittgen and Livak, 2008). n in all experiments refer to biological replicates, with two technical RT-qPCR replicates for each biological replicate. Dots represent relative gene expression of a single animal. Bars represent means ± SD of respective groups. Statistical analyses were performed using Student's t-test. *$p < 0.05$.

Tissue staining. Intestinal tissues were fixed in 4% paraformaldehyde in PBS at 4°C overnight, transferred to 70% ethanol, paraffin-embedded, and sectioned at 5 µm thickness. Paraffin-embedded sections were deparaffinized and rehydrated before staining. Antigen retrieval was performed using sodium citrate buffer (10 mM sodium citrate pH 6.0).

For immunofluorescence, the sections were blocked using BioGenex Power Block™ Universal Block Reagent at room temperature (RT) for 5 min and then incubated with primary antibody at 4°C overnight. Slides were washed three times with PBST (0.05% Tween 20 in PBS) at RT for 5 min and incubated with secondary antibody at RT for 1 h. Slides were then washed three times again with PBST and mounted by VECTASHIELD Antifade Mounting Medium with DAPI (Vector Laboratories). For immunohistochemistry, endogenous peroxidase were quenched by 3% H_2O_2 in methanol for 20 min at RT. The sections were then blocked by Avidin/Biotin and animal serum for 15 min each at RT. Then, primary antibody were incubated at 4°C overnight. Slides were washed by PBST at RT for 5 min three times and incubated with secondary antibody at RT for 0.5

h. Slides were then washed three times again by PBST and visualized via ABC and DAB reagents (Vector Laboratories). A hematoxylin counterstain was used before dehydration and mounting using Permount Mounting Medium (Fisher Scientific). For EdU detection, the Click-iT® EdU Alexa Fluor® 488 Imaging Kit (ThermoFisher Scientific) were used according to the manufacture's protocols.

Please see **Table S1** for a list of antibodies and respective dilutions. Immunofluorescent confocal images were captured using a Nikon A1-Rs confocal laser scanning microscope. Light microscopy images were captured using a Biotek Cytation 5 Imager and Plate Reader or a Nikon Ci-L Upright Microscope. All image analyses were performed using the Integrated Microscopy Core at Baylor College of Medicine.

RNA *in situ* hybridization and RNAScope®

Detection of *Axin2* mRNA by *in situ* hybridization was performed as described (Gregorieff and Clevers, 2010) on tissue fixed by immersion in 4% paraformaldehyde (PFA) in phosphate-buffered saline (PBS) for 15 minutes and embedded in Tissue-Tek O.C.T. Compound. Digoxigenin (DIG)-labeled *Axin2* antisense RNA probe was generated by *in vitro* transcription using NotI and SP6 polymerase (plasmid provided by I. Thesleff). *Wnt3* was detected on paraffin-embedded intestinal slides using RNAScope® probe 312241 following manufacturer's protocols.

SUPPLEMENTAL REFERENCES

GREGORIEFF, A. & CLEVERS, H. 2010. In situ hybridization to identify gut stem cells. *Current protocols in stem cell biology***,** 2F. 1.1-2F. 1.11.

SATO, T., VRIES, R. G., SNIPPERT, H. J., VAN DE WETERING, M., BARKER, N., STANGE, D. E., VAN ES, J. H., ABO, A., KUJALA, P., PETERS, P. J. & CLEVERS, H. 2009. Single Lgr5 stem cells build crypt-villus structures in vitro without a mesenchymal niche. *Nature,* 459**,** 262-5.

SCHMITTGEN, T. D. & LIVAK, K. J. 2008. Analyzing real-time PCR data by the comparative C(T) method. *Nat Protoc,* 3**,** 1101-8.

Figure S1.

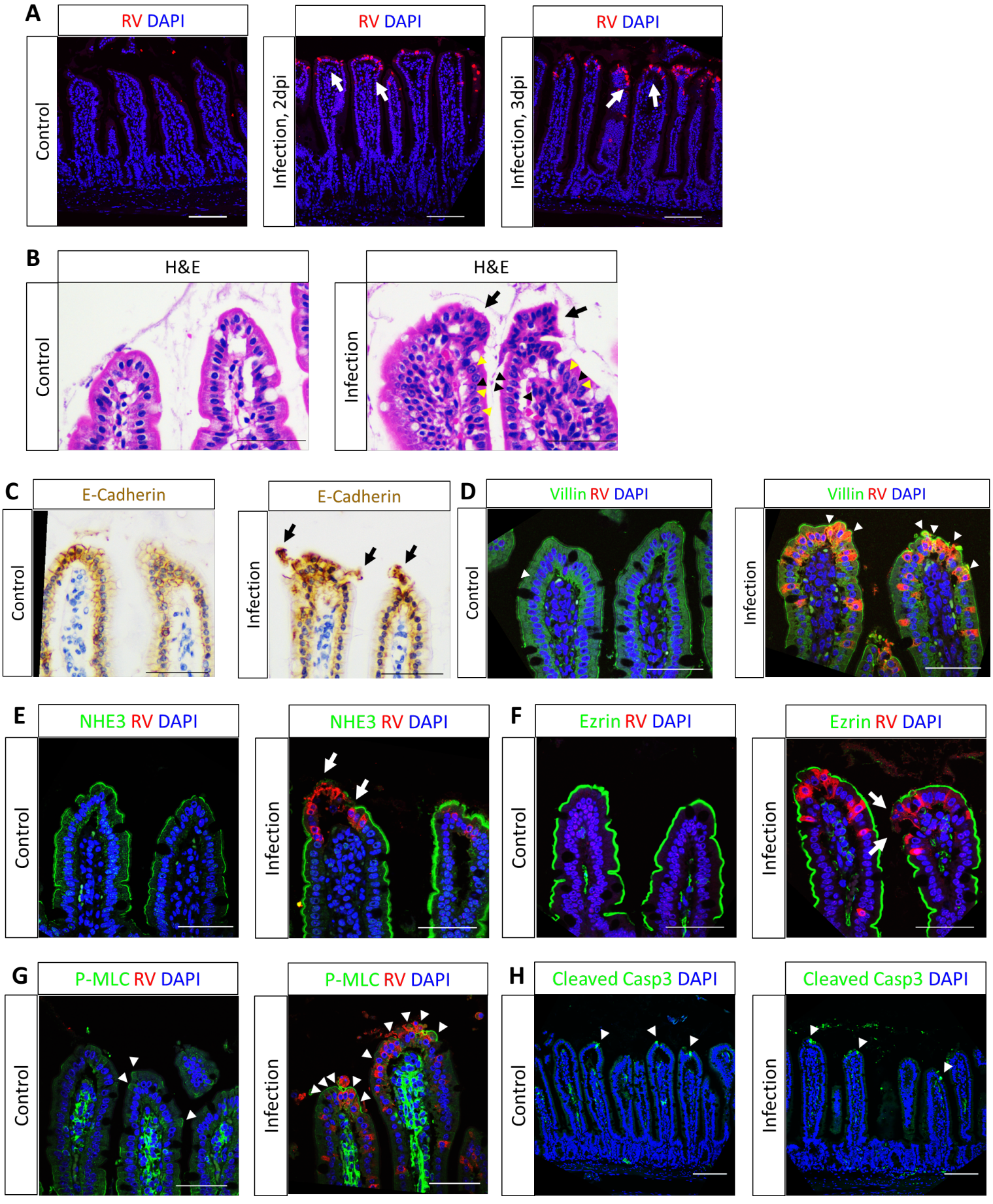
A
RV DAPI
Control
RV DAPI
Infection, 2dpi
RV DAPI
Infection, 3dpi
B
H&E
Control
H&E
Infection
C
E-Cadherin
Control
E-Cadherin
Infection
D
Villin RV DAPI
Control
Villin RV DAPI
Infection
E
NHE3 RV DAPI
Control
NHE3 RV DAPI
Infection
F
Ezrin RV DAPI
Control
Ezrin RV DAPI
Infection
G
P-MLC RV DAPI
Control
P-MLC RV DAPI
Infection
H
Cleaved Casp3 DAPI
Control
Cleaved Casp3 DAPI
Infection

Figure S1. Related to Figure 1. **RV infection causes localized damage at tips of villi. (A)** Representative confocal images of control- and RV-infected mouse epithelium at 2dpi and 3dpi. RV-infected cells are detected using a laboratory-generated, polyclonal guinea pig anti-RV antibody that detects viral structural proteins. Infected villi are noted by white arrows. **(B)** Representative H&E images of control- vs. RV-infected villi at 4dpi. Black arrows denote altered shedding at the tip of the villus. Black arrowheads denote nuclei mis-positioned either towards the apical or the basolateral surface of the cell. Yellow arrowheads denote distorted and enlarged nuclei with hypodense hematoxylin stain. **(C)** Representative immunohistochemistry staining of E-Cadherin staining in control- and RV-infected animals at 4dpi. E-Cadherin protein is mis-localized to the cytoplasm in RV-infected villus tip cells. Black arrows point to shedding cells with fragmented nuclei, indicating necrosis. **(D)** Representative confocal images of villin and RV staining in control- and RV-infected animals at 4dpi. White arrowheads denote irregular villin staining in infected villus tips with intensified villin stain on the apical cell surface and its mis-localization to the cytoplasm. **(E)** Representative confocal images of sodium–hydrogen antiporter 3 (NHE3) and RV staining in control- and RV-infected animals at 4dpi. NHE3 protein is lost in parts of RV-infected villi (white arrowheads). **(F)** Representative confocal images of ezrin and RV staining in control- and RV-infected animals at 4dpi. Ezrin protein is lost in parts of RV-infected cells (white arrowheads). **(G)** Representative confocal images of phosphorylated myosin light chain (P-MLC), a marker of anoikis, and RV staining in control- and RV-infected animals at 4dpi. P-MLC-labeled cells are increased in number following RV infection (white arrowheads). **(H)** Representative confocal images of cleaved caspase 3 (cleaved casp3), a marker of apoptosis, in control- and RV-infected animals at 4dpi. Cleaved casp3-labeled cells remained stable following RV infection (white arrowheads). Scale bars: 100 μm in A and H, 50 μm in B-G.

Figure S2.

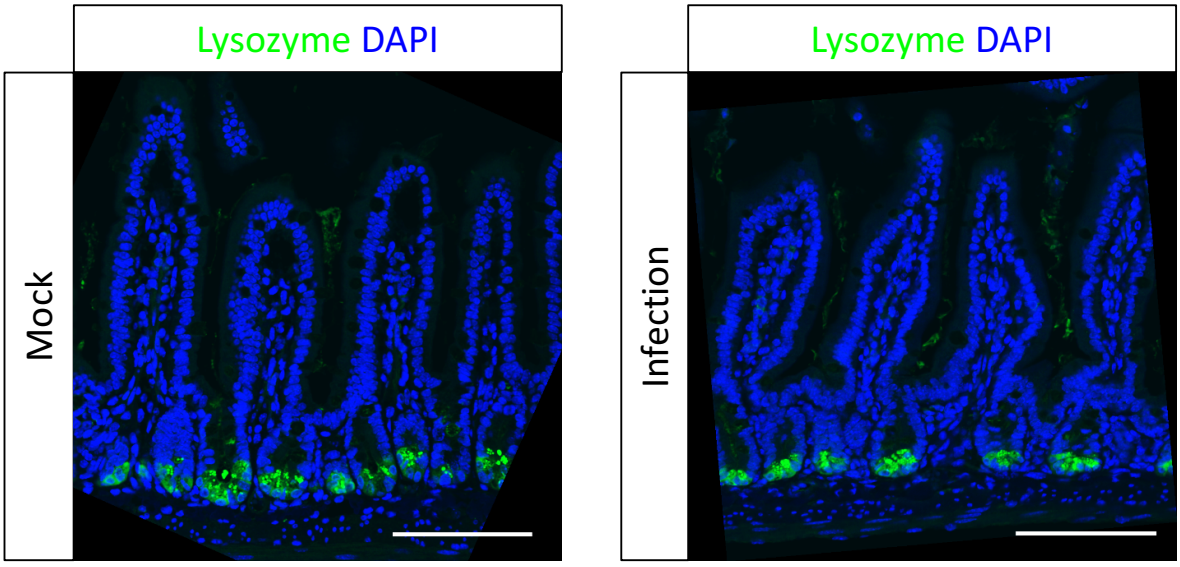

Figure S2. Related to Figure 1. **Paneth cells are intact in RV-infected animals.** Representative confocal images of lysozyme staining in control- and RV-infected animals at 4dpi. Scale bars: 100 µm.

Figure S3.

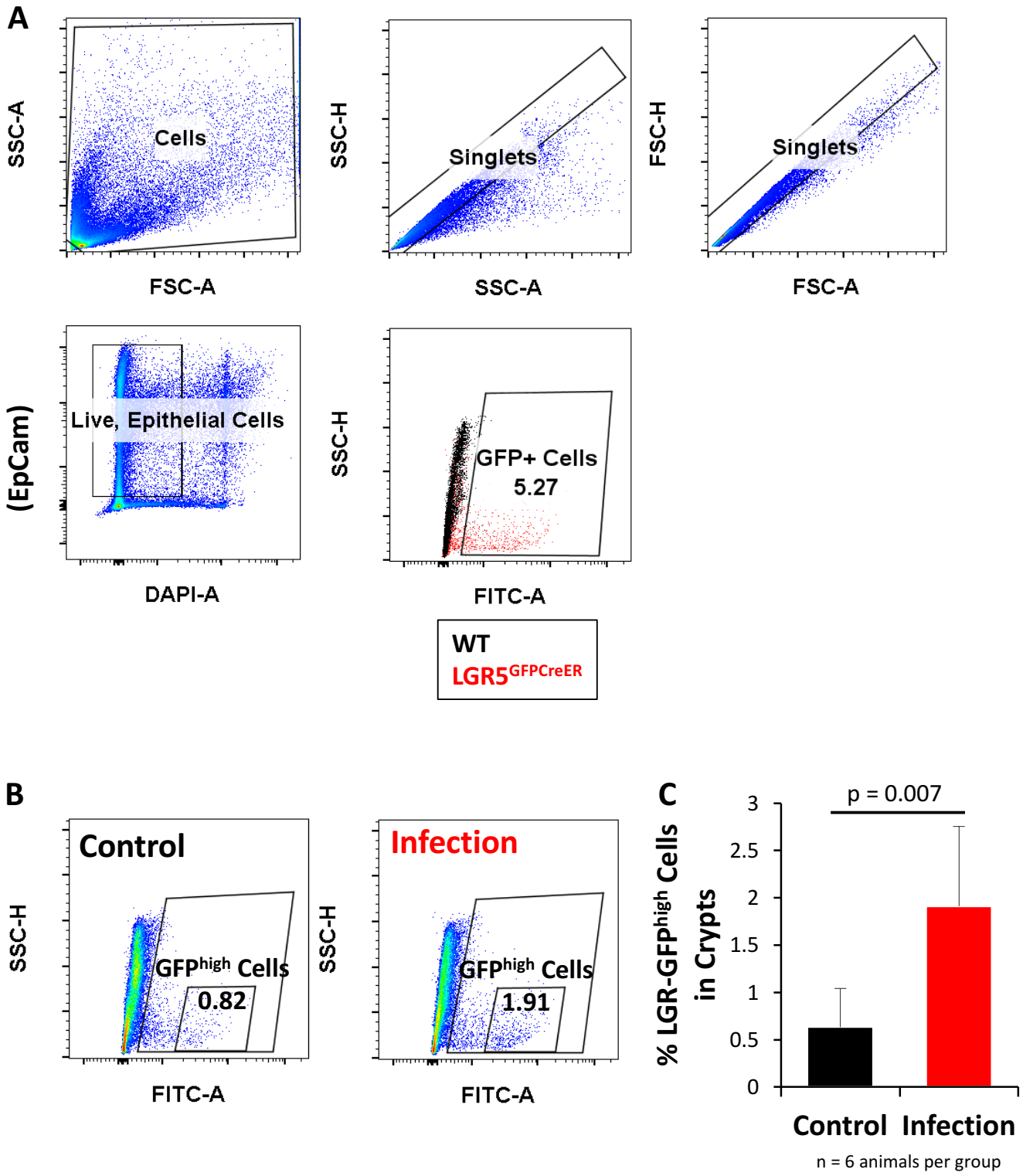

Figure S3. Related to Figure 3. **LGR5-GFP^{high} cells are increased in number following RV infection. (A)** Representative flow gating scheme for isolating viable (DAPI^{neg}), single intestinal epithelial cells (EpCAM^{pos}), then *Lgr5^{GFPCreERT}* population. All flow analysis were performed using crypt-enriched epithelial preparation. **(B)** Representative flow cytometry analysis of LGR5-GFP^{high} cell population in control- and RV-infected *LGR5^{GFPCreERT}* mice. **(C)** Quantification of LGR5-GFP^{high} cell population in control- and RV-infected animals (n= 6 mice per group with at least two independent experiments).

Figure S4.

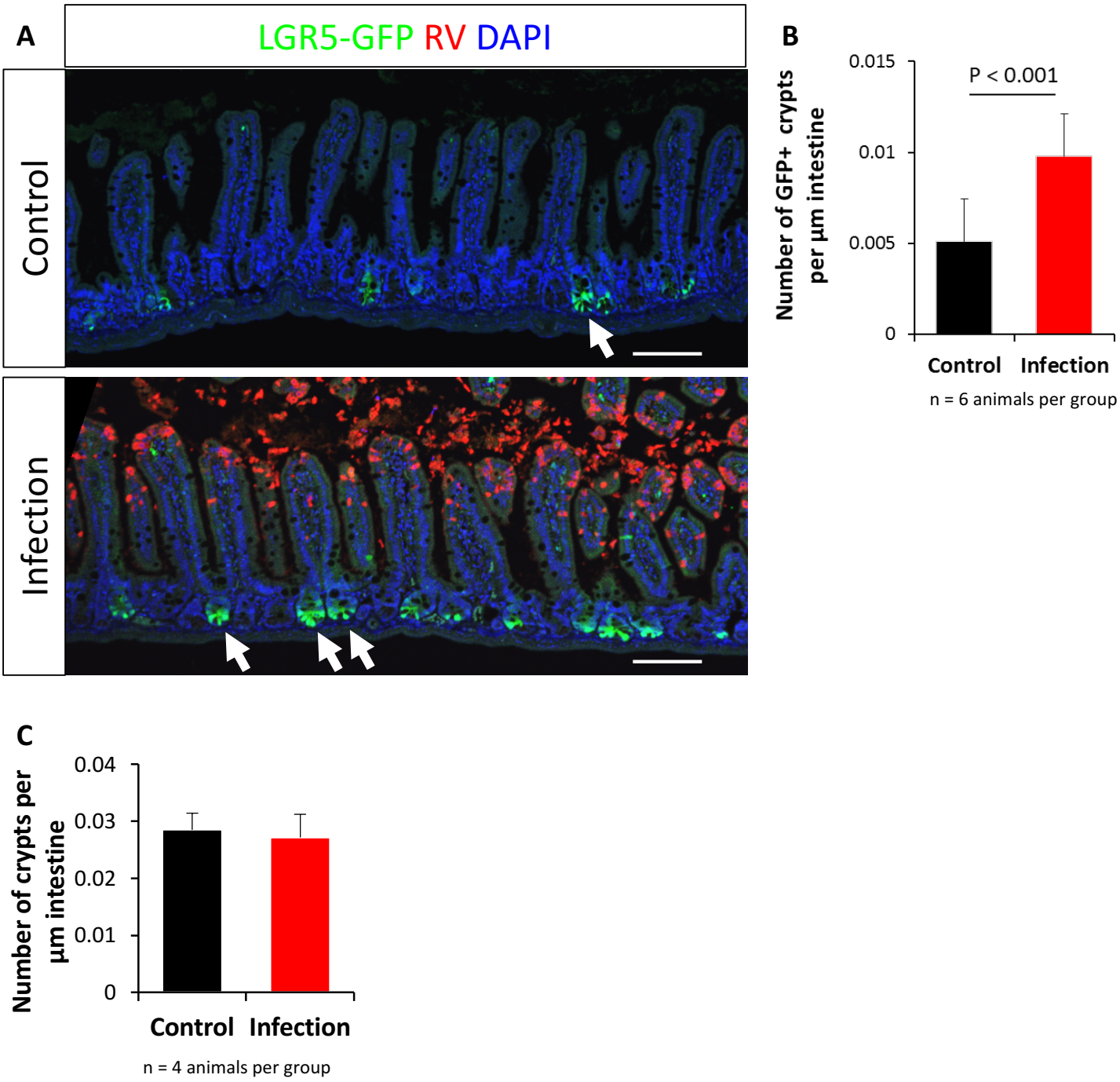

Figure S4. Related to Figure 3. **RV infection resulted in increased number of LGR5+ crypts. (A)** Representative immunofluorescent image of LGR5+ crypts in control- and RV-infected mice. Scale bar: 100 µm. **(B)** Quantification of LGR5+ crypts per µm of intestine in control- and RV-infected animals (n= 6 mice per group with at least two independent experiments). **(C)** Quantification of number of crypts per µm of intestine in control- and RV-infected animals (n= 4 mice per group with at least two independent experiments).

Figure S5.

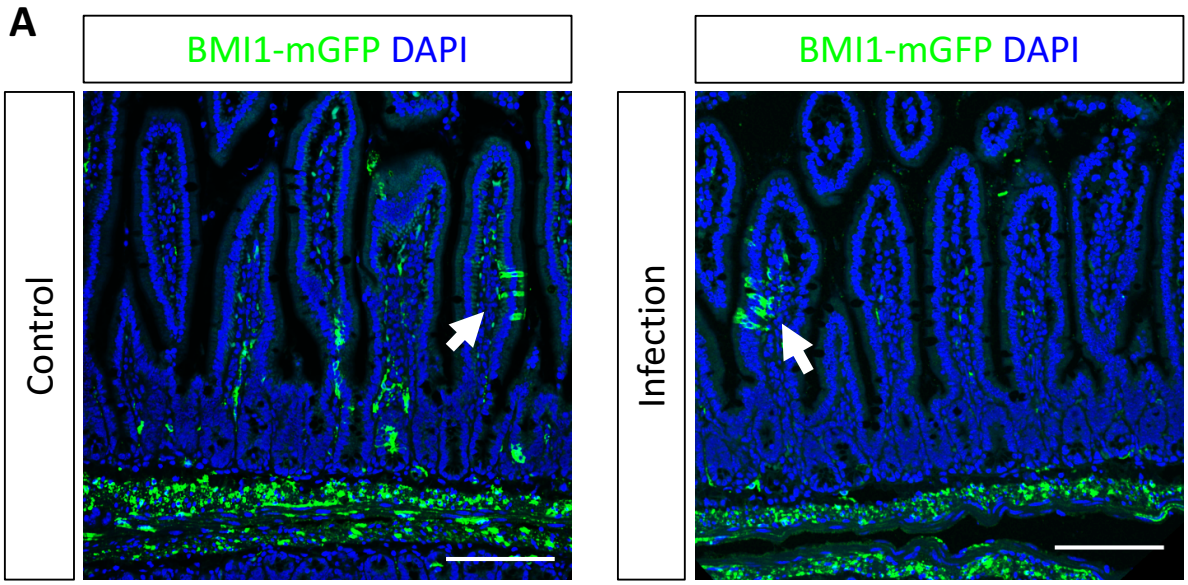

Figure S5. Related to Figure 3. **BMI1 lineage is not changed following RV infection.** Representative confocal images of *Bmi1*^{Cre};R26^{mTmG} mice 7 days after tamoxifen injection and RV infection. BMI1 lineage remained similar in control- and RV-infected animals (white arrows). Scale bar: 100 µm.

Figure S6.

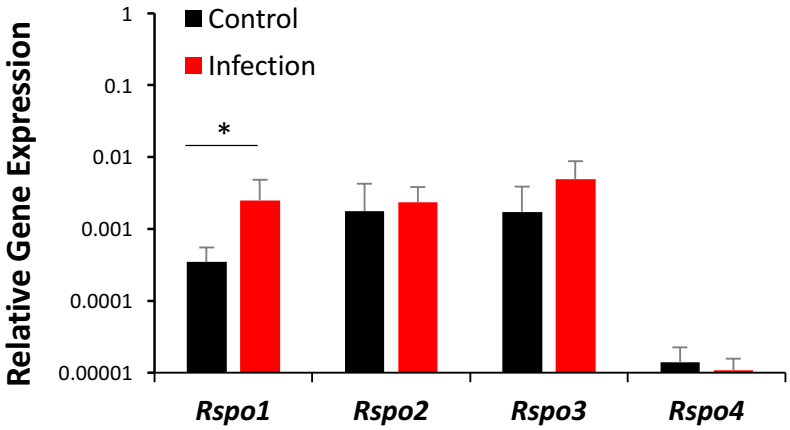

Figure S6. Related to Figure 4. **Upregulation of *R-Spondin 1* following RV infection.** RT-qPCR results showed expression of the *R-Spondin* family genes in isolated mesenchyme of WT mice following RV infection. Transcripts were normalized to *Gapdh* and relative gene expression was obtained using the $2^{-\Delta\Delta Ct}$ method (n = 3 mice per group in at least 2 independent experiments). Dots represent relative gene expression of one animal. Bars represent means ± standard deviation of respective groups. Statistical analyses were performed using Student's t-test. *$p < 0.05$.

Figure S7.

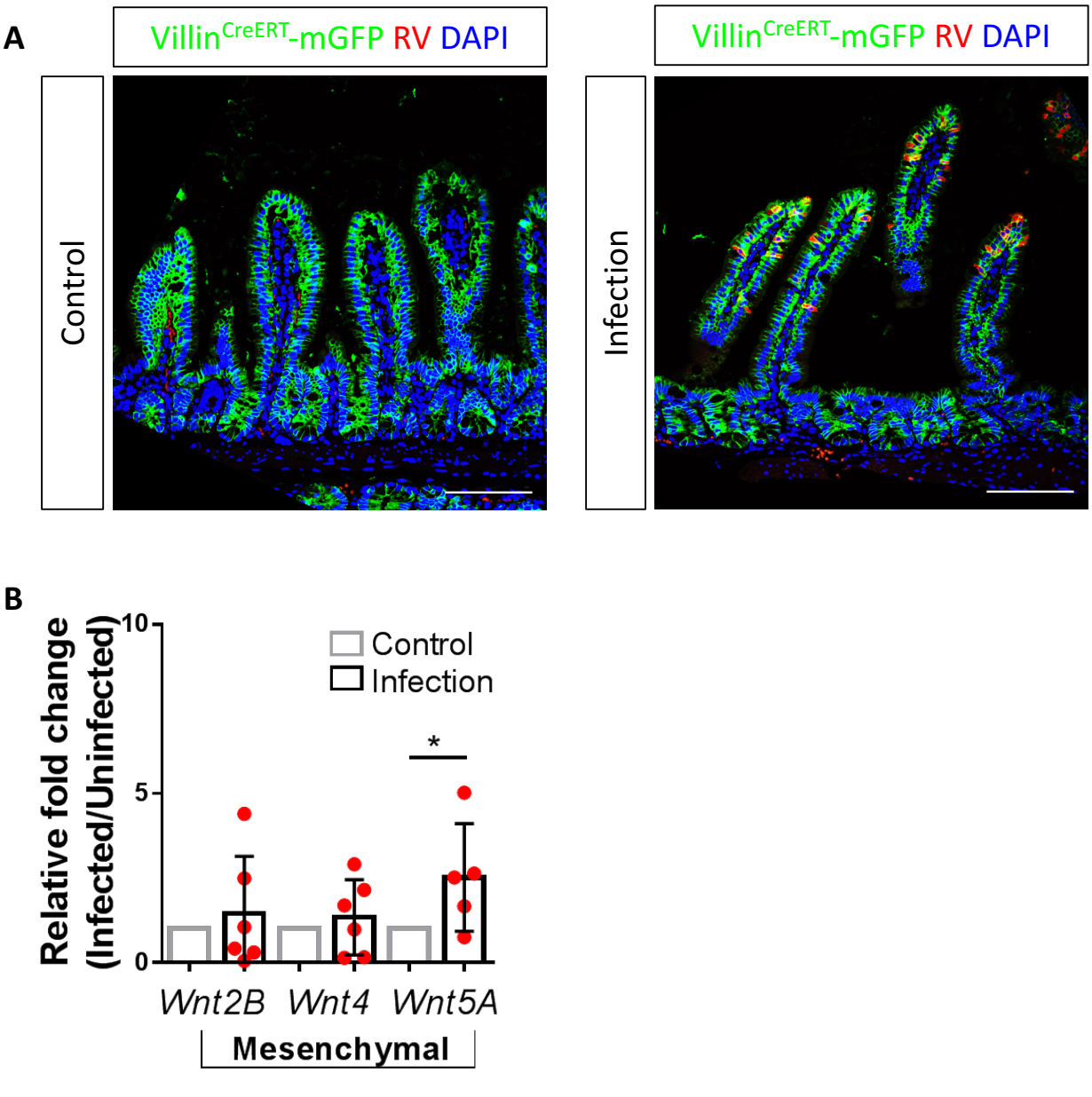

Figure S7. Related to Figure 5. **Epithelial WLS conditional KO results in mesenchymal *Wnt5A* upregulation following infection. (A)** Representative confocal images of *Villin^{CreERT};WLS$^{f/f}$;R26^{mTmG}* (WLS KO) mouse following tamoxifen injection in control and RV infection. mGFP+ cells represent epithelial cells with *Wntless* gene knockout. RV infected cells (red) visualized by guinea pig polyclonal serum that detected viral structural proteins. Scar bar: 100 µm. (B) RT-qPCR results showed expression of the mesenchymal *Wnt* family genes in isolated mesenchyme from WLS KO mice following RV infection. Transcripts were normalized to *Gapdh* and relative gene expression was obtained using the $2^{-\Delta\Delta Ct}$ method (n = 6 mice per group). Dots represent relative gene expression of one animal. Bars represent means ± standard deviation of respective groups. Statistical analyses were performed using Student's t-test. *$p < 0.05$.

Table S1. Related to Material and Methods. **Antibody information and dilutions for flow cytometry and immunofluorescence.**

Antibody	Host	Company and Catalogue no.	Dilution
EpCam/CD326	Rat	BioLegend 118213	1:200
GFP	Goat	Abcam Ab6662	1:500
Lysozyme	Rabbit	ThermoFisher 18-0039	1:1000
OLFM4	Rabbit	Cell signaling 39141	1:200
PCNA	Mouse	Cell Signaling 2586	1:500
RV (GP511)	Guinea pig	Laboratory Generated	1:200
β-catenin	Rabbit	Abcam ab32572	1:500
CC44v6	Rat	eBiosciences BMS145	1:1000
E-Cadherin	Mouse	BD 610181	1:1000
Villin	Goat	Santa Cruz sc-7672	1:500
NHE3	Rabbit	Novus NBP1-82574	1:200
Ezrin	Rabbit	Abcam ab76247	1:200
P-MLC	Rabbit	Cell Signaling 3671S	1:50
Clev. Casp. 3	Rabbit	Cell Signaling 9551	1:200

Table S2. Related to Material and Methods. **TaqMan probes used for RT-qPCR gene expression analysis.**

Gene name	Probe ID
Ascl2	Mm01268891_g1
Axin2	Mm00443610_m1
Bmi1	Mm03053308_g1
Ccnd1	Mm00432359_m1
Cd44	Mm01277161_m1
Dclk1	Mm00444950_m1
Gapdh	Mm99999915_g1
EphB2	Mm01181021_m1
Hopx	Mm00558630_m1
Ki67	Mm01278617_m1
Lgr5	Mm00438890_m1
Lrig1	Mm00456116_m1
Myc	Mm00487804_m1
Olfm4	Mm01320260_m1
Pcna	Mm00448100_g1
Sox9	Mm00448840_m1
Tert	Mm00436931_m1